7-7-2022

Tunable Passive Shock and Vibration Isolators for Rotational Isolation

Chase B. LeMaire
Louisiana State University and Agricultural and Mechanical College

TUNABLE PASSIVE SHOCK AND VIBRATION ISOLATORS FOR ROTATIONAL ISOLATION

A Thesis

Submitted to the Graduate Faculty of the
Louisiana State University and
Agricultural and Mechanical College
in partial fulfillment of the
requirements for the degree of
Master of Science

in

The Department of Mechanical and Industrial Engineering

by
Chase Bradley LeMaire
B.S.M.E., Louisiana State University, 2021
August 2022

Table of Contents

ABSTRACT III

CHAPTER 1. INTRODUCTION 1
1.1. Introduction to Vibration Isolation 1
1.2. NFL Helmet Challenge 2
1.3. Concussion Research 2
1.4. Proposed Improved Helmet Design 3

CHAPTER 2. MODELING, SIMULATION, AND OPTIMIZATION 5
2.1. Introduction 5
2.2. Methods 7
2.3. Results 16
2.4. Discussion 19

CHAPTER 3. DESIGN AND FABRICATION OF SHOCK ABSORBERS 22
3.1. Introduction 22
3.2. Methods 22
3.3. Results 26
3.4. Discussion 28

CHAPTER 4. TESTING 31
4.1. Methods 31
4.2. Results 34
4.3. Discussion 43

CHAPTER 5. CONCLUSIONS 47

APPENDIX A. SIMSCAPE MODELS AND RESPONSE OPTIMIZER 49

APPENDIX B. MATLAB CODES 54

APPENDIX C. MANUFACTURING SUPPLEMENT 64

APPENDIX D. TESTING SUPPLEMENT 67

APPENDIX E. CUSTOM TESTING MACHINE INFORMATION 70

REFERENCES 72

VITA 74

ABSTRACT

Shock and vibration isolation are a critical need in helmets, which are widely used to protect athletes, workers, soldiers, and astronauts. Passive vibration isolation systems are a good option when mass and volume should be minimized and when the experienced loadings can be predicted. However, it is frequently challenging to find materials and structures which exhibit the optimal vibration and impact isolation properties for an application. As a case study illustrating a novel design paradigm for rotational shock absorption, a family of optimal solutions for the physical properties of American football helmets is presented. Lumped parameter Simulink models simulate a variety of impacts to a helmeted head. These models were optimized to minimize the Head Injury Criterion (HIC) and Helmet Performance Score (HPS) metrics and determine the optimal values of rotational and translational stiffness and damping between the head and helmet. The optimization of the 1-dimensional simulations was validated with an analytical solution to the optimization problem. The 3-dimensional simulation suggested that a helmet optimized considering both rotational and translational accelerations could improve the Helmet Performance Score by 48% or more as compared to translational accelerations only. The optimal stiffness and damping computed from the models was used to drive the design of multi-material shock absorbing elements. A custom impact testing machine was used to test the mechanical properties of prototype isolators. A 3D printed TPU shock absorber was designed within 2.2% of the target optimal stiffness; however, no materials were found that could provide enough damping. This research illustrates a new design paradigm for independent tuning of rotational energy storage and dissipation that can be translated to a variety of applications.

CHAPTER 1. INTRODUCTION

1.1. Introduction to Vibration Isolation

There are two types of vibration isolation systems (VIS): active and passive. Active vibration isolation uses data from sensors to create feedback and feed-forward control systems in which actuators cancel-out incoming vibration. These systems are often complex and require hardware, electronics, and programming. Because of this, active VIS may not be preferred in inhospitable environments or situations where mass and/or volume should be minimized. Passive VIS on the other hand rely solely on material and geometry to absorb and dissipate the incoming energy. Because a passive system does not have the ability to adapt to the incoming excitation, passive systems require the excitation to be predictable and characterizable, so the system can be adequately designed for the application.

Passive vibration isolation and impact absorption systems have a wide range of uses ranging from space exploration applications to protective gear for sports. Some of the space applications include vibration isolation for the treadmill on the International Space Station (I.S.S.), optical stabilization for telescopes, and protection of delicate samples during the hypersonic deceleration of re-entry. These applications are shown below in Figure 1.1.

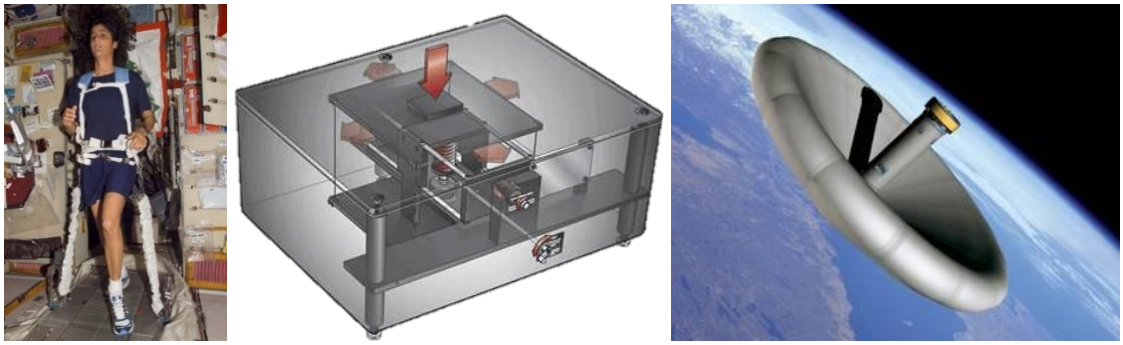

Figure 1.1. Space exploration applications for vibration isolation: I.S.S. treadmill [1] (left), MinusK vibration isolation table for sensitive instruments [2] (middle), Hypersonic deceleration [3] (right)

One of the largest active areas of impact absorption research in sports medicine is the design of helmets for the reduction of traumatic brain injuries (TBI or concussions) in American football. Brain injuries cause more deaths than any other sports-related injury with 65%-95% of football fatalities being caused by brain injuries. In any given season, 10% of college players and 20% of high school players sustain brain injuries [4].

1.2. NFL Helmet Challenge

Recent studies and films such as the 2015 movie *Concussion* have stimulated public concern and incentivized research into concussion prevention. One of the programs that incentivized this research was the NFL Helmet Challenge which offered a $1 million prize to groups that can design a new football helmet that substantially increases protection against TBIs. The NFL Helmet challenge has a well-defined test protocol and uses standardized performance metrics for helmets. These metrics quantify the helmet performance and lend themselves to optimization which is beneficial in the design process. For these reasons, the NFL Helmet Challenge has been chosen as a case study to demonstrate the design and fabrication of optimally tuned shock absorbers.

1.3. Concussion Research

TBIs are largely caused by the pressure and shear forces from the inertial accelerations experienced during an impact. The brain is suspended in cerebral fluid inside of the skull. When the skull experiences a rapid acceleration due to an impact, the inertia of the brain causes its movement to lag the movement of the skull. When accelerations are large enough, this lag can cause the brain to impact the interior of the skull, damaging the brain tissue [5]. There are two components of this acceleration –translational and rotational. Translational accelerations cause spikes in pressure in the brain which have been shown to correlate with the peak neurologic

dysfunction; however, studies have shown that the highly organized brain tissue is even more sensitive to the shear forces caused by rotational accelerations. This is because the brain strain (deformation) induced by the shear forces is much larger than the strain induced by pressure gradients [6]. One severe form of TBI is Diffuse Axonal Injury (DAI) which results from a blunt injury to the brain that causes disconnection or malfunction of neurons' interconnection. An estimated 10% of all TBI patients admitted to the hospital have some degree of DAI as well, and of these DAI cases, it is estimated that 25% will result in death [7].

1.4. Proposed Improved Helmet Design

Football helmet designs typically address the translational accelerations; however, research indicates that the shear forces caused by rotational accelerations are the predominant mechanism of injury. This research proposes a new helmet design, shown in Figure 1.2, that addresses both translational and rotational aspects of a collision.

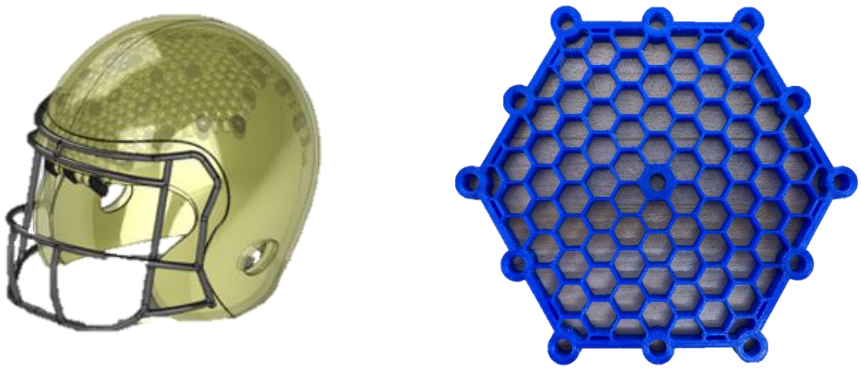

Figure 1.2. Proposed helmet design (left), Single hexagonal shock element (right)

The new design consists of two helmet shells. The inner shell is largely unaltered from existing designs with foam on the inside to cushion the head and dissipate energy resulting from translational accelerations. While the foam on the inside of the inner shell can shear which would allow relative head-helmet rotation, the head is connected nearly rigidly to the inner shell via the chinstrap. Any rotation of the inner shell gets transferred directly to the head and vice-versa, preventing any significant relative rotation between the head and the inner shell. Between the

inner shell and the outer shell is an energy dissipating layer made up of a network of optimized hexagonal shock absorbers. The inner shell will be fixed to the head via a chin strap causing the kinematics of the head and the inner shell to be coupled. The energy dissipating layer between the shells, however, allows for differential rotation between the outer shell and the head which can isolate the head and reduce its rotational acceleration. The shock absorbers are designed to provide the optimal response that minimizes the effects of rotational accelerations on the brain.

The following chapters explore the design of the energy dissipating layer which is the first step of making this proposed design a reality. The optimal properties of the energy dissipating layer can be determined through modeling and simulation. These optimal mechanical properties then become targets that must be achieved through the design and fabrication of shock absorbing elements. These shock absorbing elements should be tested to verify the mechanical properties before moving on to the final stage of assembling a working helmet prototype.

CHAPTER 2. MODELING, SIMULATION, AND OPTIMIZATION

2.1. Introduction

The problem at hand is a constrained optimization intended to minimize the Head Injury Criterion (HIC) performance metric given an allowable maximum displacement. The optimal solution to this impact problem has been solved analytically by Balandin et al. [8]

Consider a lumped mass m with displacement x subject to the differential equation and initial conditions

$$m\ddot{x} = u, \tag{1}$$

$$x(0) = 0, \ \dot{x}(0) = v_0 \tag{2}$$

Define an optimal control problem (the primal problem) to choose $u(t)$ such that the final displacement $x(T)$ is minimized subject to a constant value of the HIC function evaluated on the acceleration $\ddot{x}$. Formally, this is the minimization of the function

$$J_1 = \max_{t\in[0,\infty)} |x(t)| \tag{3}$$

The HIC function may be defined as

$$J_2 = \max_{t_2-t_1\leq\Delta} \left\{ \left[\frac{1}{t_2 - t_1} \int_{t_1}^{t_2} \frac{|u(t)|}{m} dt \right]^{2.5} (t_2 - t_1) \right\} \tag{4}$$

The primal problem of minimizing $x(T)$ subject to $J_2 \leq H$ by choosing the function $u(t)$ has been solved by Balandin et al. [8]. Define the dimensionless parameters

$$\hat{x} = \frac{H^{2/3}}{v_0^{8/3}} x, \ \ \hat{t} = \frac{H^{2/3}}{v_0^{5/3}} t, \ \ \hat{u} = \frac{u}{m} \left(\frac{v_0}{H} \right)^{2/3} \tag{5}$$

$$\widehat{\Delta} = \frac{H^{2/3}}{v_0^{5/3}} \Delta, \ \ \widehat{J_1} = \frac{H^{2/3}}{v_0^{8/3}} J_1, \ \ \widehat{J_2} = \frac{1}{H} J_2 \tag{6}$$

For the region of interest in the impact problem for Helmets, the optimal solution is given by

$$\hat{u}(t) = \begin{cases} -\frac{3}{5}\hat{t}^{-2/5} & \hat{t} \leq 1 \\ 0 & \hat{t} > 1 \end{cases} \tag{7}$$

The maximum displacement is $\widehat{J_2} = 3/8$, v_0 is the impact velocity, and H is the allowed Head Injury Criterion (HIC) which is defined in section 2.2. The optimal value of J_1 for each restriction $J_2 \leq H$ may be plotted on a two-dimensional graph of J_1 and J_2, which form the Pareto frontier for the problem (see Figure 2.1 for an example). Note that HIC increases substantially with velocity. For example, at an initial velocity of 5 m/s, the optimal HIC value for a maximum displacement of 25 mm is approximately 124, while for an initial velocity of 6 m/s, the optimal HIC value for a maximum displacement of 25 mm is approximately 250. An example of the analytical optimal force input $u_0(t)$ is shown in Figure 2.6 as a red dashed line.

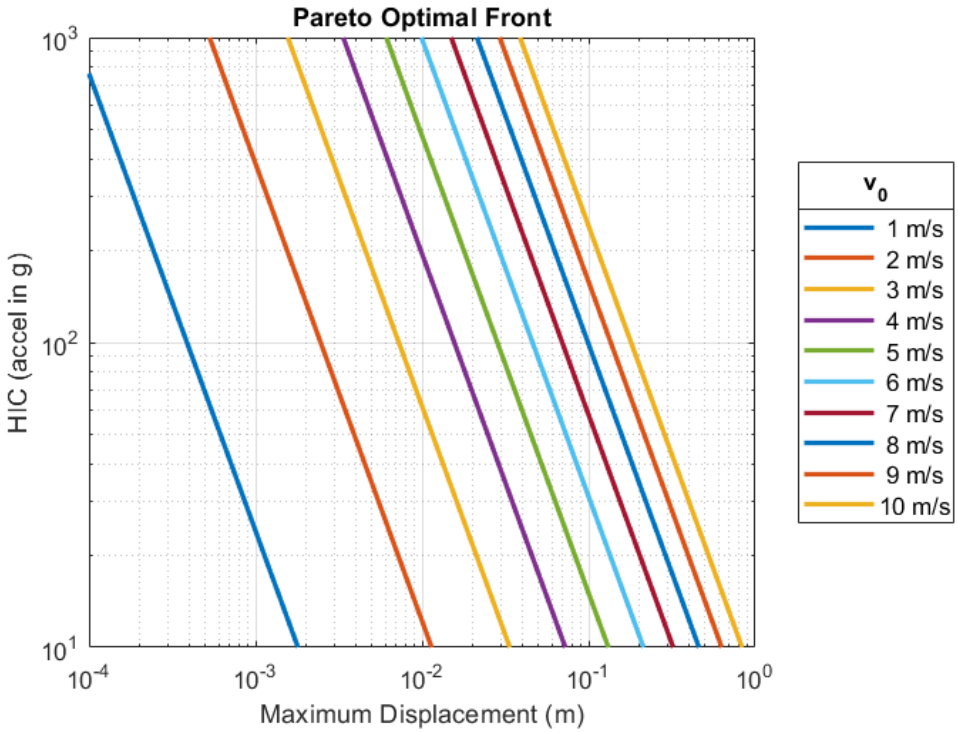

Figure 2.1. Pareto frontier for maximum displacement vs. HIC value for a single-mass, linear impact model. Each curve corresponds to a specific initial velocity in m/s. The slope of the constant v_0 line on the log-log plot is -1.5.

The dual problem to the primal problem is to select the optimal u to minimize the HIC functional under the constraint of a fixed maximum bound $x(T) \leq x_{max}$, as would be found in many practical applications such as the impact absorption using a fixed amount of space to take up the impact. The solution to the primal problem, which could be denoted as a function $x_{max} = \Phi(H; v_0, \Delta)$. The relationship between x_{max} and H is monotonic (as H increases, x_{max} decreases). As a result, the optimal u for the dual problem is the same as for the solution to the primal problem, and we need only to look up the solution to the primal problem which happened to satisfy the bound $x(T) = x_{max}$ as the inverse function with the same v_0 and Δ, $H = \Phi^{-1}(x_{max}; v_0, \Delta)$. This is equivalent to the statement that the axes on Figure 2.1 can be flipped, which is obvious given the shape of the graph.

Note that any solution that falls outside of the curve in Figure 2.1 (that is, further from the origin) is not optimal, because either the maximum displacement or the HIC could be lowered. Solutions on the line are optimal in one of the senses described by the primal and dual problems. Solutions below the lines are not feasible points. This means that they are not achievable by any impact absorbing system, passive or active.

2.2. Methods

2.2.1. 1-D Modeling Methods

Several different metrics are used to quantify the performance of the football helmets. These standard metrics were derived by Biocore LLC [9] and are the standard method of assessing helmet performance for the NFL Helmet Challenge testing protocol. The first metric is the Head Injury Criterion (HIC) which is a measure of the translational accelerations of the head during an impact. Note that the acceleration must be in units of “g”.

$$HIC = \max_{t_2 - t_1 < \Delta} \left\{ \left[\frac{1}{t_2 - t_1} \int_{t_1}^{t_2} a(t)\, dt \right]^{2.5} (t_2 - t_1) \right\} \tag{8}$$

The second metric is called DAMAGE which is a function of the rotational accelerations during impact. DAMAGE stands for "Diffuse Axonal Multi-Axis General Evaluation," and it predicts maximum brain strain using the angular accelerations time-histories from a head impact [10]. The DAMAGE metric was provided by the NFL Helmet Challenge as a MATLAB function. This function can be viewed in Appendix B. The weighted combination of these two metrics creates the Head Acceleration Response Metric (HARM). The weights were determined by fitting the equation to the experimental test data of dummy reconstructions of on-field football impacts.

$$HARM = 0.0148(HIC) + 15.6(DAMAGE) \tag{9}$$

The test protocol includes 18 different impact conditions. The HARM scores resulting from each of these tests can be combined into an overall Helmet Performance Score (HPS).

$$HPS = \sum_{i=1}^{18} M_i (HARM)_i \tag{10}$$

The weighting factors for each test condition (M_i) were calculated such that the overall contribution of each impact condition is reflective of the on-field concussion incidence. Table 2.1 below summarizes the weighting factors for the HPS. [9]

Table 2.1. Weighting factors (M_i) for each test condition used for calculating Helmet Performance Score (HPS) [9]

Impact Location	5.5 m/s	7.4 m/s	9.3 m/s
Side Upper (SU)	0.0293	0.0182	0.0233
Oblique Front (OF)	0.00949	0.00601	0.00782
Oblique Rear (D)	0.00583	0.00371	0.00472
Side (C)	0.00996	0.00624	0.00813
Facemask Side (FMS)	0.00392	0.00258	0.00358
Facemask Central Oblique (FMCO)	0.00687	0.00493	0.00687

Modeling was performed in Simscape using the Multibody toolbox. Simscape is part of the Simulink environment but uses blocks that represent physical elements rather than Simulink's state space modeling language. Simulink's Response Optimizer application was used to determine the stiffness and damping parameters that optimize a helmet performance metric.

The first model created was a linear, single degree of freedom (1-DOF) mass, spring, damper system. A linear spring and damper were in parallel between a mass and a ground reference state. An ideal translational motion sensor was in parallel with the spring and damper and measured the displacement of the shock absorber. An ideal force sensor was in series with the system and measured the force transmitted through the shock absorber. Figure 2.2 below shows the linear impact model.

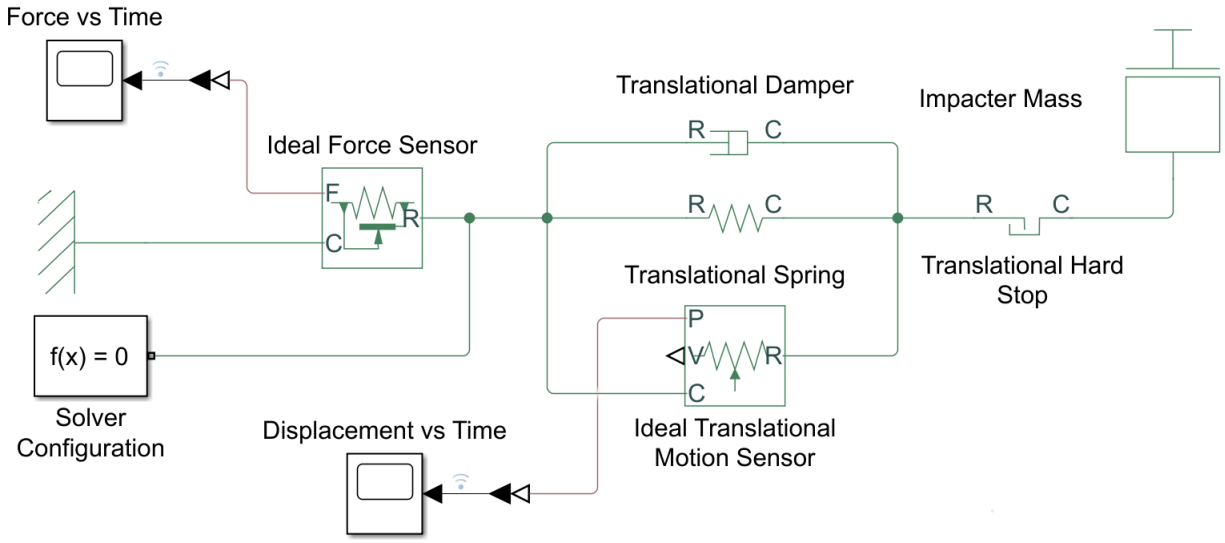

Figure 2.2. Kelvin-Voigt viscoelastic material model.

The second model used the same 1-D linear element model, but the mass spring damper system was allowed to slide rather than being fixed directly to the mechanical ground. This was to simulate the head which, according to the testing protocol, is allowed to slide on a track after impact. This model is shown below in Figure 2.3.

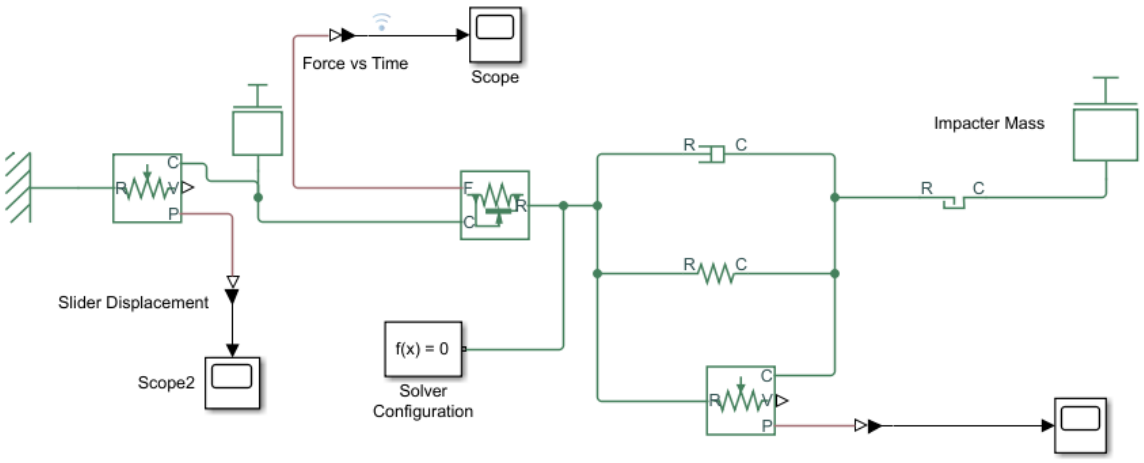

Figure 2.3. Linear impact Simscape model with sliding capability

The third model used the Maxwell model of viscoelasticity (spring and damper in series) in parallel with another spring. This configuration is often referred to as the Zener Dashpot model and is shown below in Figure 2.4. As the spring labeled “k2” becomes increasingly stiff, that element begins to approximate a stiff rod and the Maxwell model approaches the Kelvin-Voigt model. Simulink’s ODE15s variable step solver was used. The translational hard stop used in previous models caused simulation issues and had to be removed to be solvable across the optimization region. A condition was implemented to stop the simulation at the first zero-crossing of the contact force between the impacting mass and the shock absorber. The contact force equaling zero is indicative of the point of separation of the impact mass from the shock absorber. Stopping the simulation at this point avoids oscillations due to the inertia of the attached mass in the model since this is not the idealized behavior of the system being modeled. One limitation of this method is that the deformation lags the force response due to the damper. This means that the simulation stops before the deformation can return to zero. This is not a problem since the optimization uses only force data in the minimization of the HIC objective function. The maximum displacement signal bound is still an effective constraint in the

optimization. After optimization, simulations were run without the zero-crossing stop condition to ensure that the displacement eventually returned to zero.

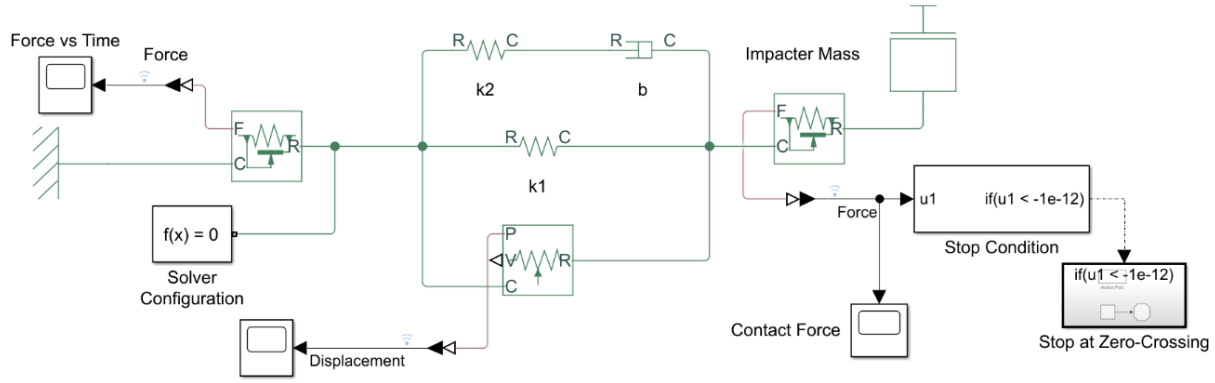

Figure 2.4. Maxwell representation of the Zener dashpot model for viscoelastic materials

The optimization of all three of these 1D models was performed using Simulink's Response Optimizer application. Let J_1 be the maximum displacement as defined in Equation 3 and J_2 be the HIC performance metric defined in Equation 8. Let $p = (k_1, k_2, b)$. Then the following optimization problem is defined:

$$p^* = \arg\min_p J_2 \quad (11)$$
$$subject\ to$$
$$J1 \leq x_{max}$$
$$\dot{x} = v_0$$
$$x(0) = 0$$

Parallel computing was enabled to allow the optimizer to use all four (4) cores of the computer to run simulations which quadrupled optimization speed. The optimization of the 1D model generally completed within 30 minutes with some optimizations taking less than 5 minutes.

2.2.2. 3D Modeling Methods

The fourth model replicates the full 3D impact scenario of the test protocol with all 6 DOF (3 translational and 3 rotational). This model is a lumped parameter model meaning all sources of stiffness and damping between the head and helmet are combined into a single overall

stiffness and a single overall damping. The impact geometry is a sphere approximating the Schutt Air XP geometry. The geometry of the face mask is not explicitly modeled. It is considered an impact surface which is rigidly attached to the helmet shell.

The head is modeled as a rigid body with a mass of 10 lbm (4.54 kg) per General Motors (GM) drawings [11] for the Hybrid III dummy and mass moments of inertia as measured by Kaleps [12]. The center of mass location relative to the neck was taken from the original GM drawings. The geometric shape was extracted from the finite element model codes provided by Biocore, LLC [9]. The 6 DOF joint that represents the movement of the helmet relative to the head can be defined with unique translational stiffness and damping coefficients in each of the 3 axes and a single global rotational stiffness and damping coefficient. This model used the same translational stiffness and damping coefficients along each axis to reduce optimization complexity resulting in a total of 4 design variables for the optimization: translational stiffness, translational damping, rotational stiffness, and rotational damping.

This model also includes an estimated stiffness of the artificial neck that is used on the helmet testing apparatus. The neck is modeled using the general beam element provided as a default element in Mathworks Simscape, which uses Euler-Bernoulli theory for bending and axial deformations and the Saint-Venant theory for torsion. The beam has a length of 4.875”, matching the original GM drawings for the flexible section of the neck, and a diameter of 2.51”. The length is divided into 4 discrete beam elements. The flexural rigidity of the neck is tuned using the material modulus so that the response to a modeled certification test per 49 CFR 572 results in a passing certification for total head rotation in flexion [11]. The damping coefficient was set to achieve a damping ratio of approximately 0.2 calculated by the logarithmic decrement method. The neck model does not exhibit the asymmetric flexion/extension response displayed

by the real dummy. In addition, the head is modeled as rigidly attached to the superior end of the neck, i.e. without any model of the "nodding blocks" in the HIII dummy. The full 6 DOF model can be seen in Figure A.1 in Appendix A.

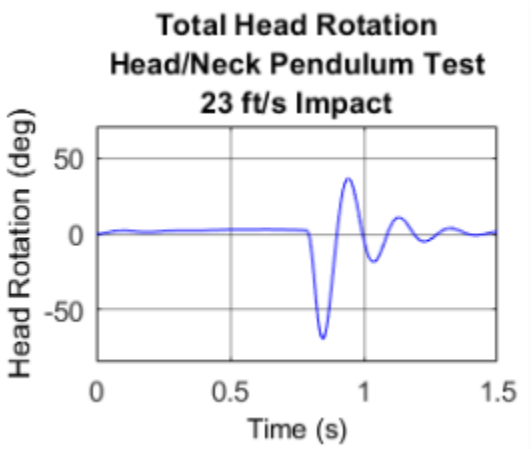

Figure 2.5. Validation result based on the definitions of 49 CFR 572. Peak head rotation is 69°, occurring 61ms after impact.

MATLAB's Response Optimizer application was used to determine the combination of stiffness and damping parameters that would yield the lowest (best) HPS when subjected to all 18 impact conditions of the test protocol. Let J_1 be the maximum translational displacement, J_2 be the maximum rotational displacement, and J_3 be the HPS as defined by equation 10. Let $p = (k, b, k_r, b_r)$ which are the translational and rotational stiffness and damping coefficients. Define the optimization problem as:

$$p^* = \arg\min_p J_3 \qquad (12)$$
$$subject\ to$$
$$J_1 \leq x_{max}$$
$$J_2 \leq \theta_{max}$$
$$\dot{x}(0) = v_0, \quad x(0) = 0$$
$$\dot{\theta}(0) = 0, \quad \theta(0) = 0$$

To understand how the HPS varies across a range of displacement constraints, several combinations of constraints were tested. The combinations of constraints were selected using a central composite design [13] which intends to span the range of acceptable displacements while

minimizing cross correlation trends between the variables. The HPS was plotted as a function of the two allowable displacements and a least-squares surface regression was performed on the data set to estimate the trend. A contour plot was also created using the same data to show level set HPS curves on a 2-D plane. From this contour plot, a suitable combination of displacement bounds was selected and an optimization was run with these bounds to generate the necessary translational and rotational stiffness and damping coefficients.

2.2.3. Conversion of Rotational to In-plane Parameters

The translational parameters will mainly be taken care of by the layer of foam inside of the inner shell of the helmet. The rotational parameters, however, will be achieved with the second shell and the network of hexagonal shocks. In order to use these parameters to drive the design of the individual hexagonal shock absorber elements, these values must be converted into in-plane stiffness and damping values. Using spherical coordinates to parameterize a sphere with radius R

$$\begin{aligned} x &= R\sin\theta\cos\phi \\ y &= R\sin\theta\sin\phi \\ z &= R\cos\theta \end{aligned} \tag{13}$$

On the surface of the sphere, the surface element has the form

$$dA = R^2\sin\theta\, d\theta\, d\phi \tag{14}$$

For an angular unit virtual displacement $\delta\vec{k}$, the virtual displacement at the surface of a unit sphere is described in spherical coordinates as

$$\delta\vec{x}(\theta,\phi) = \delta\vec{k} \times \vec{r}(\theta,\phi) \tag{15}$$

Considering that the virtual displacement is larger on the points of the sphere further from the axis of rotation, the effective displacement factor is defined so that the mean virtual displacement $\overline{\delta x}$ under a unit angular virtual displacement is $R\overline{\Delta}$. The factor $\overline{\Delta}$ is the areal mean of the virtual displacement divided by the radius R.

$$\bar{\Delta} = \frac{\overline{\delta x}}{R} = \frac{1}{4\pi R^2}\int \frac{\|\delta\vec{x}\|}{R}\, dA \tag{16}$$

The cross product has magnitude

$$\|\delta\vec{x}\| = \left\|\delta\vec{k}\right\|\|\vec{r}\| \sin\angle\left(\delta\vec{k},\vec{r}\right) = R\sin\angle(\delta\vec{k},\vec{r}) \tag{17}$$

By symmetry, the orientation of $\delta\vec{k}$ may not change the result $\bar{\Delta}$. Select $\delta\vec{k} = \vec{e}_z$ for the sake of computation so that $\angle\left(\delta\vec{k},\vec{r}\right) = \theta$. Then

$$\bar{\Delta} = \frac{1}{4\pi R^3}\int R^3 \sin^2\theta\, d\theta\, d\phi = \frac{\pi}{4} \approx 0.785 \tag{18}$$

The effective radius for a distributed translational stiffness located along a sphere of radius R from the centroid of the spherical joint is therefore $R_e = \bar{\Delta}R$. If the distributed stiffness is located at the actual radius $R_a = 100$ mm, the effective radius is $R_e = 0.785(100\text{ mm}) = 78.5$ mm. The total in-plane stiffness of all shock absorber elements located at the effective radius R_e is

$$k_{\text{tot}} = \frac{1}{R_e^2}k_R \tag{19}$$

If there are $N = 9$ shock absorber elements in parallel distributed uniformly over the spherical surface, the in-plane stiffness of each element must be

$$k = \frac{1}{N}k_{\text{tot}} \tag{20}$$

The in-plane rotational damping is computed in the same way where the total and individual in-plane damping are respectively given by

$$b_{\text{tot}} = \frac{1}{R_e^2}b_R \tag{21}$$

$$b = \frac{1}{N}b_{tot} \tag{22}$$

2.3. Results

The optimization of the 1-D model agrees with the analytical solution of Balandin et. al [8]. The simulated optimal force response depicts the same characteristic sharp peak followed by a rapid decay to zero. The optimal analytical and simulated force responses are shown below in Figure 2.6 alongside the simulated displacement responses.

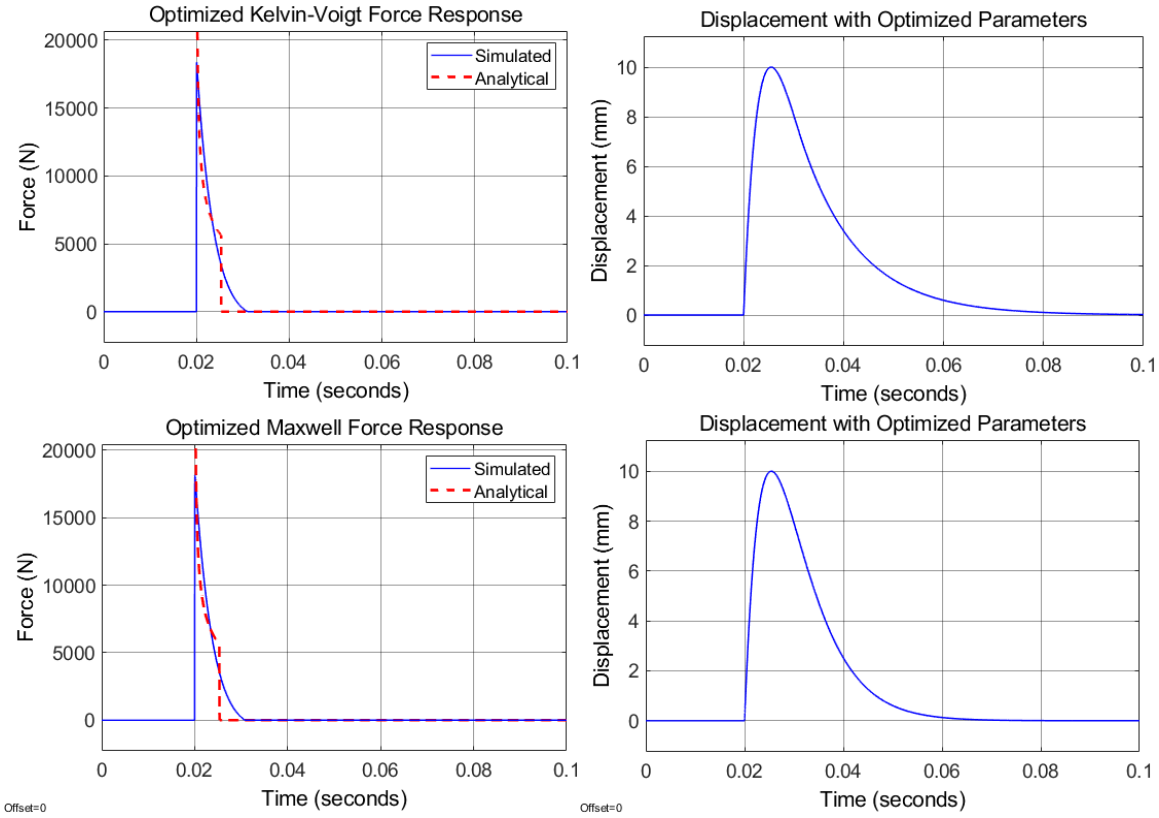

Figure 2.6. Optimum force and displacement responses for 10 mm allowable displacement and 5 m/s impact velocity: Kelvin-Voigt model (top), Maxwell model (bottom)

The minimal Head Injury Criterion (HIC) was simulated for a few impact conditions and compared to the analytical solution. The results are summarized in Table 2.2.

Table 2.2. Analytical versus simulated optimal HIC scores

Allowed Displacement	Impactor Velocity	Analytical Target HIC	Kelvin-Voigt HIC (% error)	Maxwell HIC (% error)
10 mm	3 m/s	61.7	63.88 (3.5%)	70.5 (14.3%)
10 mm	5 m/s	476.2	522 (9.6%)	538 (13.0%)
20 mm	4 m/s	69.0	74.62 (8.1%)	77.7 (12.6%)
30 mm	6 m/s	190.0	210.14 (10.6%)	215.2 (13.3%)

The remaining results are for the 3-D modeling. The least-squares surface regression on the optimized HPS data set is shown below in Figure 2.7.

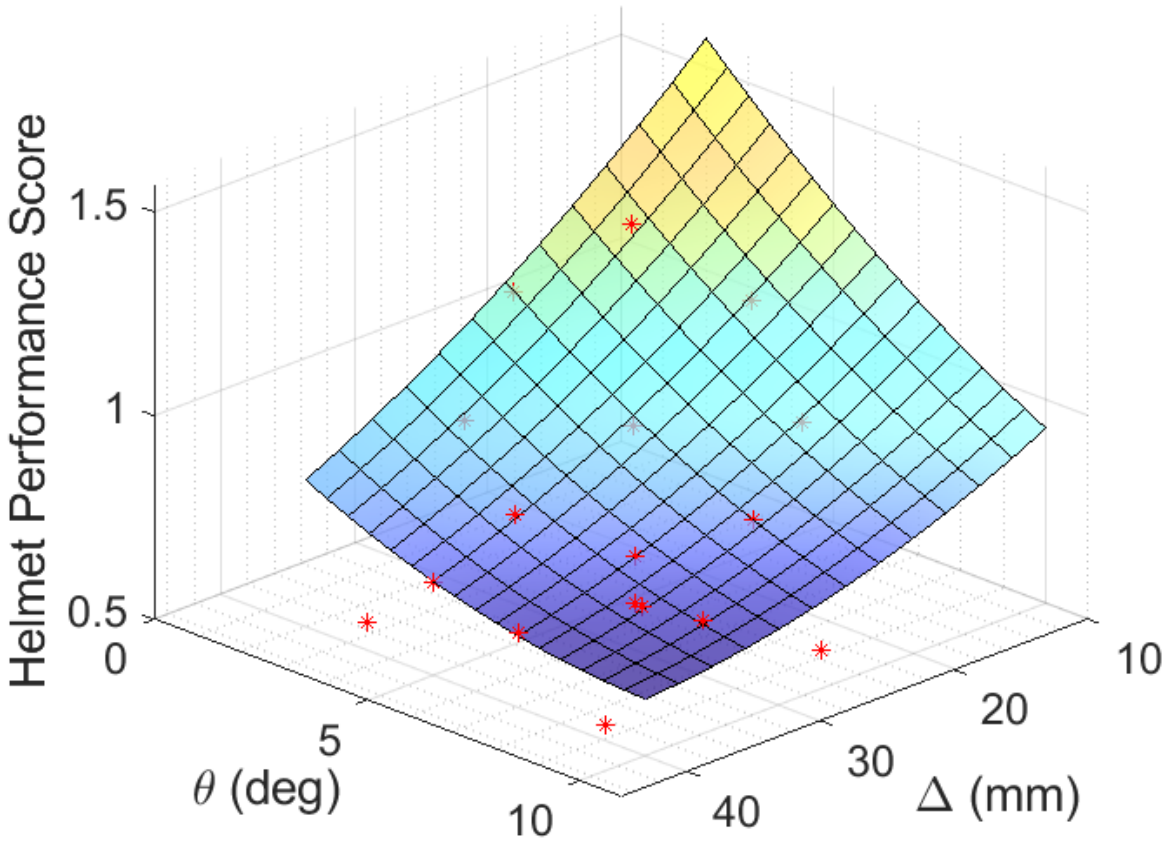

Figure 2.7. 3-D Optimization surface regression. The red asterisks indicate the optimized HPS raw data.

A contour plot was generated from the same data set. The level set curve of the 0.7 target HPS is shown. The red circles are the data points used for the regression.

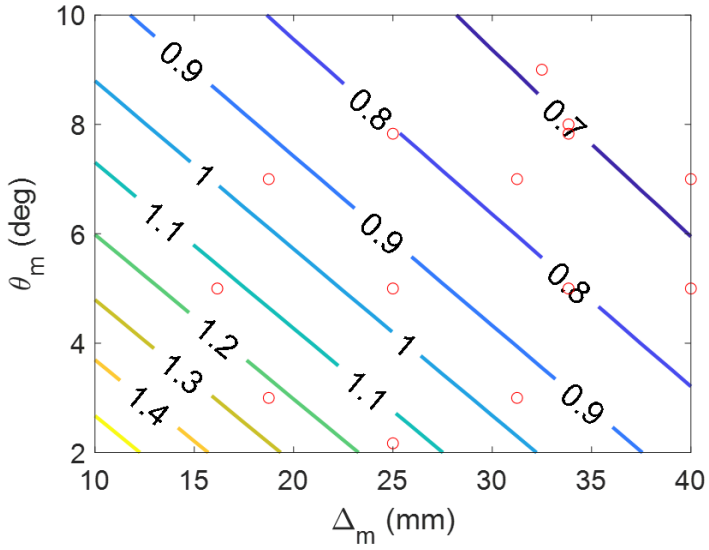

Figure 2.8. Contour plot on 3-D optimization data

A combination of 32.5 mm and 9° was selected as the combination of bounds that would yield a HPS of 0.7, the target set by the NFL Helmet Challenge. An optimization was run with these displacement bounds, and the necessary stiffness and damping parameters were computed. These parameters are shown in Table 2.3 below. The in-plane rotational values are computed from the rotational parameters as detailed in section 2.2.3 and become the target values for the shock absorber design.

Table 2.3. Optimized stiffness and damping resulting from a 32.5 mm allowed translation and 9° allowed rotation

	Stiffness	Damping
Translational	$42700\frac{N}{m}$	$1300\frac{N\,s}{m}$
Rotational	$1100\frac{N\,m}{rad}$	$32\frac{N\,m\,s}{rad}$
In-plane Rotational (Target)	$19800\frac{N}{m}$	$580\frac{N\,s}{m}$

When a full helmet test protocol (18 impact conditions) was simulated with the optimized stiffness and damping parameters, the HPS was calculated to be 0.69. The rotational freedom

was then removed from the model by setting the rotational stiffness to a large value ($1e12\,\frac{N\,m}{rad}$) and the full test protocol was simulated again. The HPS increased to 1.33.

2.4. Discussion

2.4.1. 1-D Simulation and Optimization

The intuitive prediction of the optimal force response may be to limit the force to a smaller magnitude over a longer time; however, this was not the conclusion of the analytical nor the simulated solutions. This intuition is true when the displacement is not constrained, but it does not hold for this application when the displacement is limited to just a few centimeters. If a larger displacement was allowed, the transfer of energy could happen over a longer distance which would lower the maximum force; however, because the allowable displacement is only a few centimeters, this transfer of energy must happen quickly resulting in a large and immediate peak force. Because the HIC performance metric penalizes periods of high accelerations (forces), it follows that the optimal response would attempt to lower the acceleration magnitude as quickly as possible. The resulting response is a large peak with an immediate and rapid decay.

The simulated HIC scores of the Kelvin-Voigt model were all within about 10% of the analytical solutions while the percent error of the Zener model was always 3-11% more than the analogous K-V model. It's important to note that no optimization yielded a HIC score lower than the analytical optimal solution. This would suggest an impossible outcome. The K-V model demonstrated reliable and accurate predictions of the minimum HIC score for a given combination of allowable displacement and impact velocity which suggested that the simulation and optimization techniques used could be applied to the optimization of the 3D model.

The optimization of the Kelvin-Voigt model was more accurate than the optimization of the Zener model when comparing minimized HIC scores. This suggests that a parallel spring and

damper can more accurately model the optimal solution than the Zener model. The K-V material model was maintained in the 1D sliding model and the 3D modeling.

The 1-D results presented were generated using only linear spring and damping elements. Of course, no spring or damper is truly linear in practice. Nonlinear spring and damping elements were explored but caused the computational load and solve time to increase substantially. Nonlinear spring elements are defined by force and displacement vectors while nonlinear damping elements are defined by force and velocity vectors. This increased the number of optimization variables by a factor of N-1 where N is the length of each vector. Consider the scenario where the nonlinearity of the spring and damper are defined by 1x9 vectors that span positive and negative numbers and include the origin. Excluding the origin from the optimization, this would yield 8 free design variables for each element, or 16 total free parameters to be optimized. In contrast, a model with linear spring and damper elements would only have 2 free parameters for optimization, the spring constant and damping coefficient. The optimization for the nonlinear model was far more computationally intensive and did not yield any improvement in accuracy over the linear element model when compared to the analytical solution. Linear elements were used for all subsequent models.

2.4.2. 3-D Simulation and Optimization

Figure 2.7 shows the trend for the relationship of HPS as a function of the translational and rotational displacement bounds. The HPS increases rapidly as both displacements decrease which is an analogous trend to the one observed with the 1-D relationship as shown in the Pareto optimal front in Figure 2.1. This surface regression allows for a reversal in the way these problems are addressed. Rather than choosing displacements and solving for the optimal HPS, a target HPS can be selected, and the figure will suggest combinations of displacement bounds that

can achieve the target HPS. A target HPS of 0.7 is desired because that will outperform all existing helmets per communication from NFL Helmet Challenge personnel. There exists an infinite number of displacement combinations that will yield this HPS, but 32.5 mm of translational displacement and 9° of rotation were selected because both of these values are attainable and within the design and performance requirements of the helmet. These properties shown in Table 2.3 are global values due to the nature of the lumped parameter model.

The simulated HPS of 0.69 achieved the target of 0.7 set by the NFL Helmet Challenge. It is hypothesized that this goal would be realized by a helmet with the optimized translational and rotational stiffness and damping coefficients of Table 2.3. This HPS with rotational freedom (0.69) was 48% lower (better) than the same model without the rotational freedom (1.33). This significant improvement in the simulated performance of the helmet indicates the importance of helmet designs that address both the translational and rotational accelerations experienced during a collision.

CHAPTER 3. DESIGN AND FABRICATION OF SHOCK ABSORBERS

3.1. Introduction

Even with the optimal stiffness and damping known, the challenge of achieving these parameters with real materials and geometries remains. This is one of the largest limitations of passive vibrations isolation systems. Even if a material has the desired stiffness, it is unlikely that it also possesses the desired damping, and vice versa. This challenge can be addressed using a combination of materials, one supplying the stiffness and one supplying the damping. If materials are chosen in such a way that the stiff material has minimal damping and the damped material has low stiffness, then changing the amount of one material will only have meaningful effects on one property. This decoupling of the stiffness and damping parameters allows for independent tuning of the properties and allows for highly customizable shock absorbers.

This research intends to address the rotational aspects of collisions; however, the shock absorbers will be designed and analyzed in a linear sense using an in-plane stiffness and damping. An in-plane analysis of the shock absorbers simplifies the modeling, manufacturing, and testing of the shocks. The conversion of rotational parameters to the analogous in-plane parameters is detailed in section 2.2.3.

3.2. Methods

3.2.1. Material Selection

The backbone or “skeleton” of the shock absorber must provide the stiffness and elasticity for the shock absorber. A range of rubbers were considered for this application. Rapid prototyping of various designs would be essential to the testing intensive approach that would be taken in designing the shock absorbers. This limited the material selected to flexible 3D printable filaments. Thermoplastic polyurethane (TPU) was selected as the material because it is common,

easily obtained, has a high elastic range, and there are many online resources for printing help. Creality TPU was the first type of TPU tested, but it was harder and stiffer than desired for the application. NinjaTek NinjaFlex TPU was much more elastic, had a lower hardness of Shore 85A, and had better printability. NinjaFlex in the Sapphire Blue color was selected. It is frequently observed that material properties of the same type of filament vary with material color [14], so the Sapphire Blue color was kept consistent in all prints.

The damping material must have low stiffness to minimize effects on the stiffness of the shock and must withstand the inhospitable environment of a football helmet. A closed-cell flexible foam was chosen to avoid absorbing perspiration and becoming heavy. The material should also be easily shaped to take the form of the voids among the rubber backbone of the shock absorber. FlexFoam-iT! 6 made by Smooth-On was chosen to test as one possible damping material. This is a two-part, closed-cell, flexible, and castable foam.

It was later discovered that this choice of foam had poor damping qualities and alternative solutions were explored. Sorbothane was chosen to explore its superior damping properties. Sorbothane is advertised as one of the most highly damped materials on the market claiming up to 94% of impact energy absorption. Sorbothane has been implemented for various impact absorption and vibration isolation applications such as the treadmill on the International Space Station, camera stabilization on the space shuttle, and even sporting equipment like baseball gloves [15].

3.2.2. Manufacturing Methods

The TPU structure of the shock absorber was printed on a Dremel 3D45 printer. This printer has a direct drive extruder which is essential for printing flexible filaments like NinjaFlex. Flexible filaments do not have enough rigidity to effectively be driven through a

Bowden tube and into the extruder. Direct drive extruders are mounted to the print head which minimizes the length of the filament between the drive motor and the nozzle and improves extrusion. In all prints except one, the TPU had sufficient adhesion to the glass print bed on its own and did not require any other form of adhesive such as glue. All models were imported as an STL file and sliced using the Dremel slicer software version 1.2.3.

Twelve (12) different honeycomb pattern designs were created with varying wall thicknesses and cell sizes. The diagram below labels the “cell size” and “wall thickness” dimensions for reference.

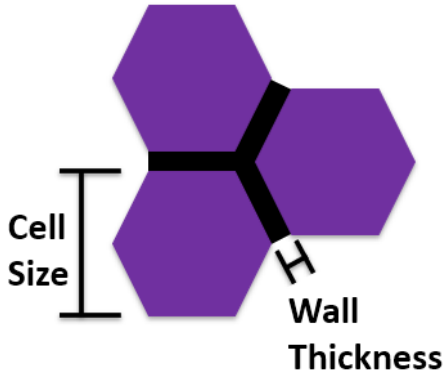

Figure 3.1. Wall thickness and cell size dimension diagram

The naming convention for the shock absorbers is based on these two dimensions and is shown in Figure 3.2.

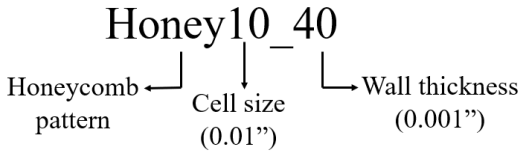

Figure 3.2. Naming convention for shock absorbers

Filling the voids (honeycomb cells) of the shocks with foam posed an interesting challenge. A basin was 3D printed so that the hex shocks fit snuggly inside and 3D printed pins were inserted into the pin holes of the shock absorber to prevent foam from filling those areas. The basin was hot glued to a plexiglass plate. A synthetic grease was used on the plexiglass

plates to reduce the adhesion of the foam and aid in removal of the sample after curing. The foam was made by pouring equal parts of Part A and Part B in a cup and stirring with a popsicle stick until thoroughly mixed. The mixture was then poured into the basin and allowed to spread evenly along the bottom. The hex shock was then pressed into the basin of liquid and the foam was allowed to expand and rise through the shock to fill the voids. A plexiglass plate was placed on top to ensure a smooth surface finish on both sides. Holes were pre-drilled in the top plate at the location of each void to allow any excess foam to overflow. Both plates were clamped together until the foam cured. The pot life of the foam is only 30 seconds so adequate preparation of materials is vital to a successful application of foam. See Appendix C for more details on the Basin Method and Figure C.1 specifically for a visual of the setup.

The liquid, castable form of Sorbothane is not sold, so 12”x12” sheets of Sorbothane were purchased instead. The desired patterns were waterjet out of the sheets. The 30-durometer variety of Sorbothane was selected to minimize the contribution to the overall shock absorber stiffness.

3.3. Results

3.3.1. Printing of Hexagonal Shock Absorbers

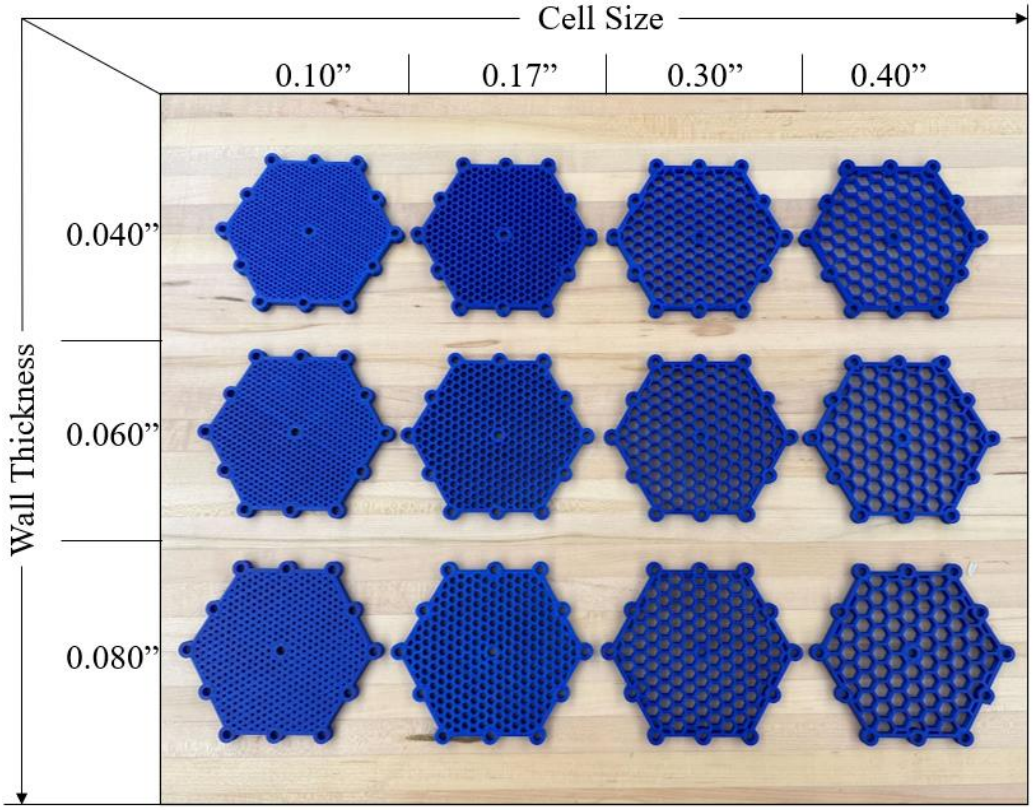

Figure 3.3. 3D printed hexagonal shock absorbers

3.3.2. Flex-Foam iT!

A copy of the honey40_40 sample was filled with foam. The process distorted the shape of some of the individual honeycomb cells. However, each cell was successfully filled with foam and a smooth top and bottom surface of the foam was achieved. The foam-filled hexagonal shock is shown in Figure 3.4.

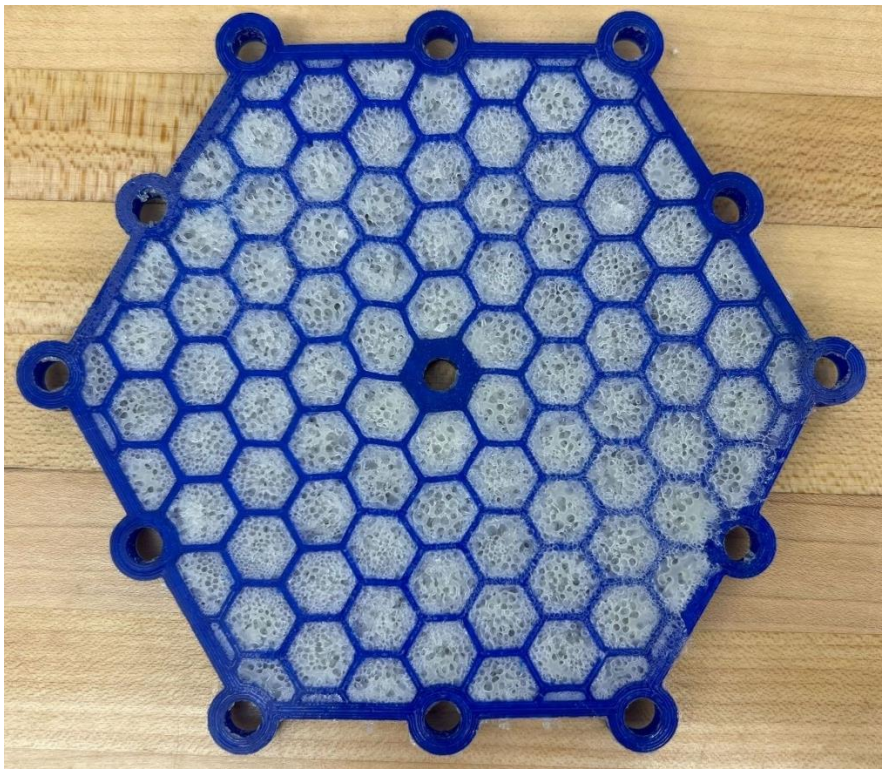

Figure 3.4. Honey40_40 filled with FlexFoam iT! 6

3.3.3. Sorbothane

The Sorbothane sheets were cut on the waterjet. Two hex shock patterns were cut: a solid (no honeycomb) pattern and the honey40_40 design. These are the stiffest and least stiff designs respectively and would give an achievable range of stiffnesses and indicate whether the target stiffness is even achievable with this material and geometry. Both patterns are shown below in Figure 3.5.

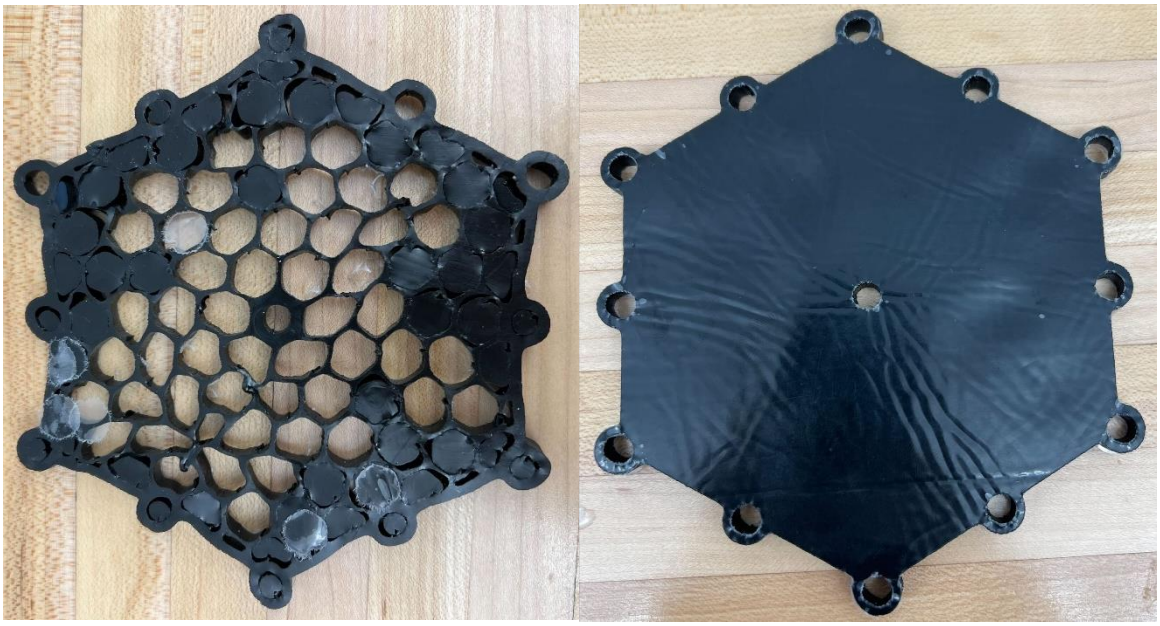

Figure 3.5. Waterjet Sorbothane samples: honey40_40 (left) and solid (right)

3.4. Discussion

3.4.1. Printing of Hexagonal Shock Absorbers

Regarding 3D printing TPU, the printing parameters were tailored to address the tendency of TPU to leak from the nozzle which leads to unintentional extrusion during travel causing excessive stringing and messy prints. This was minimized through manipulation of the printing temperature, retraction, and the “Combing” option being set to “All”. The temperature must be hot enough to melt the filament, but a temperature too high will lower the viscosity of the molten plastic too much and increase leaking from the nozzle tip. Retraction during travel sometimes causes jamming when using flexible filaments, but it is helpful in reducing leaking. A low retraction distance and speed were set to reduce leaking while avoiding jamming that could be caused by large retractions. The “Combing” option restricts the travel paths to be contained within the print area. Any material that leaks from the nozzle is contained within the interior of the print which prevents the strings and unwanted material in the travel paths.

The print times of the TPU shocks were very large due to the slow print speed required for the material. The shortest print took approximately 12 hours while the longest print took approximately 33 hours. The prints with the 0.060” and 0.080” wall thicknesses were of better quality than the 0.040” wall thickness because the combing option was ineffective on the small wall thicknesses. The slicer was unable to restrict the travel paths to the thin walls of the part which caused travel paths to cross honeycomb cells leading to an increase in stringing.

3.4.2. Flex Foam-iT!

The distortion of the walls in the foam filled sample could be due to either the clamping force or due to an inequal amount of foam in each cell. Ideally, each cell would have an identical amount of foam and the forces of the expanding foam would be equal and opposite on each side of the wall. It is unlikely that the expanding foam could generate enough force to create the significant deformations observed. It is more likely that the clamping of the plexiglass plates caused the sample to deform or buckle under the load.

The synthetic grease prevented virtually all adhesion of the foam to the plexiglass which allowed for an easy removal of the clamping plates. The 3D printed pins prevented foam from entering the pin holes in the sample. There was some leakage observed between honeycomb cells over the top surface of the shock that resulted from inadequately distributed pressure on the top plate. This leaked foam has no impact on the properties of the sample and is purely an aesthetic problem. This could be avoided in the future by having more clamping locations on the top plate.

3.4.3. Sorbothane

Sorbothane did not provide adequate rigidity and would deform under contact with the jet of water leading to imprecise cuts. The material was too soft to get the detail of intricate patterns. The hexagonal cutouts of each honeycomb ended up being nearly circular instead (likely due to

the precision of the waterjet machine) and the walls between the honeycombs were inconsistent thicknesses (due to the sample moving while cutting). The sample itself was not stiff enough to overcome the adhesion of its own surfaces to restore its shape, rendering the sample useless.

The solid sample was good quality and was able to be tested. The plastic sheets that covered the top and bottom surfaces of the sample were kept on during testing to prevent the surfaces from sticking to the top or bottom plates of the testing machine's sample holder (Figure 4.2).

Sorbothane was a difficult material to work with, but that could be improved in a few different ways. Since viscosity has a direct variation with temperature, a colder material would be more rigid. Freezing the Sorbothane may improve its ability to be waterjet and lead to a higher quality sample. Sorbothane is a sticky material which is not conducive to this application for a couple reasons. First, the adhesive forces between the surfaces are often too much for the sample to overcome preventing the material from returning to its original shape. Additionally, friction between the sample and the sample holder could skew the damping measurement. The addition of talc power (baby powder) to the surface could reduce these excessive adhesion problems.

CHAPTER 4. TESTING

4.1. Methods

4.1.1. TPU Test Prints

A simplified geometry was used as a test sample to evaluate the quality of the print under various printing parameters. The simplified geometry could be printed in a fraction of the time of the full sample and used significantly less material. The test geometry contained all the features of the full print which gave a sufficient prediction of the quality that could be expected from a print of the full hexagonal shock. The test geometry is shown below in Figure 4.1. This model contains a pin hole and 0.4” honeycomb cells with 0.040” wall thickness, all the features that make up the full hexagonal shock. As previously mentioned, the patterns with the 0.040” wall thickness posed the largest challenge for the printer, so printing parameters that work well for this geometry were expected to work even better for the other patterns.

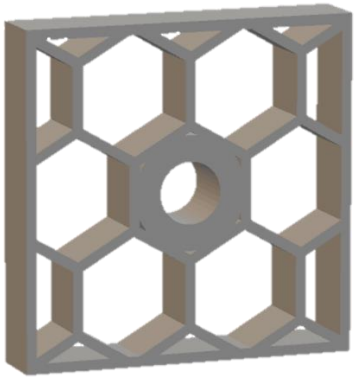

Figure 4.1. Test print geometry based on the honey40_40 pattern

4.1.2. Stiffness and Damping Testing

A custom impact testing machine was designed by Noble Plastics (see Figure 4.2). This machine uses a pneumatic actuator to compress springs and launch an impactor mass down a sliding rail where it passes through a pair of photogates and impacts the shock absorber sample. The hex shock is secured to the bottom of the sample holder via 12 pins equally spaced along the

perimeter. A pin is screwed through the top plate of the sample holder and into the center hole of the sample. The bottom plate is analogous to the inner shell of the helmet while the top plate is analogous to the outer shell. A Linear Variable Differential Transformer (LVDT) measures the displacement of the sample during impact (relative displacement between the top and bottom plates) and a load cell measures the transmitted force. Images of this machine are shown below in Figure 4.2.

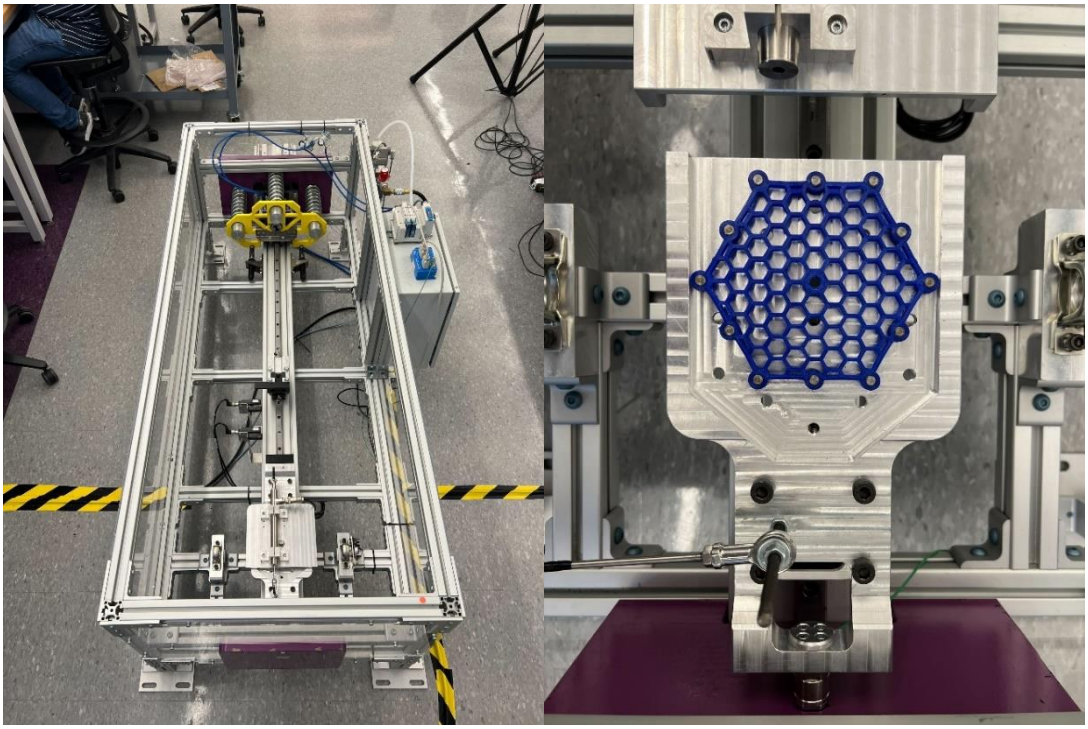

Figure 4.2. Impact testing machine (left). Sample holder with hexagonal shock (right)

A LabView program was used to control the machine as well as log, display, and automatically save the force, displacement, and impact velocity data. A screenshot of the front panel of this LabView program is shown in Figure D.2 in Appendix D.

As standard least-squares regression was performed on the force and displacement data. The impact data was fit to an $F = kx + bv$ model which estimated the stiffness and damping coefficients. Define the regressor matrix

$$\Phi = [v, x] \tag{23}$$

where x and v are column vectors of the displacement and velocity (obtained from the forward differentiation of the displacement data). Let $\theta = [b, k]^T$ where k and b are the stiffness and damping coefficients, respectively. The model can be rewritten in matrix form as

$$F = \Phi\theta \tag{24}$$

and the estimated stiffness and damping coefficients

$$\hat{\theta} = \left[\hat{b}, \hat{k}\right]^T = (\Phi^T\Phi)^{-1}\Phi^T F \tag{25}$$

A MATLAB function called *fit_model* was used to perform this least-squares regression. The forward differentiation of the displacement magnified the small oscillations in the displacement data set which created an erratic velocity signal. MATLAB's *filtfilt* command was used on the velocity to remove some of the high frequency "noise", leaving the desired signal intact for the regression. The *filtfilt* command filters signals twice: once forwards and then once in reverse to cancel out the phase shift. The *fit_model* function can be found in Appendix B.

The computed stiffness and damping coefficients were plotted on a 3D graph versus the cell size and wall thickness. MATLAB's curve fitting toolbox was used to create an interpolant cubic surface regression on the data points. The cubic interpolation provided a smooth, continuous, and monotonic trend.

4.2. Results

4.2.1. TPU Test Prints

Six (6) different test samples were printed. The quality of each print was evaluated and used to adjust the printing parameters slightly for the subsequent print until a satisfactory quality was achieved. The six samples are shown below in Figure 4.3.

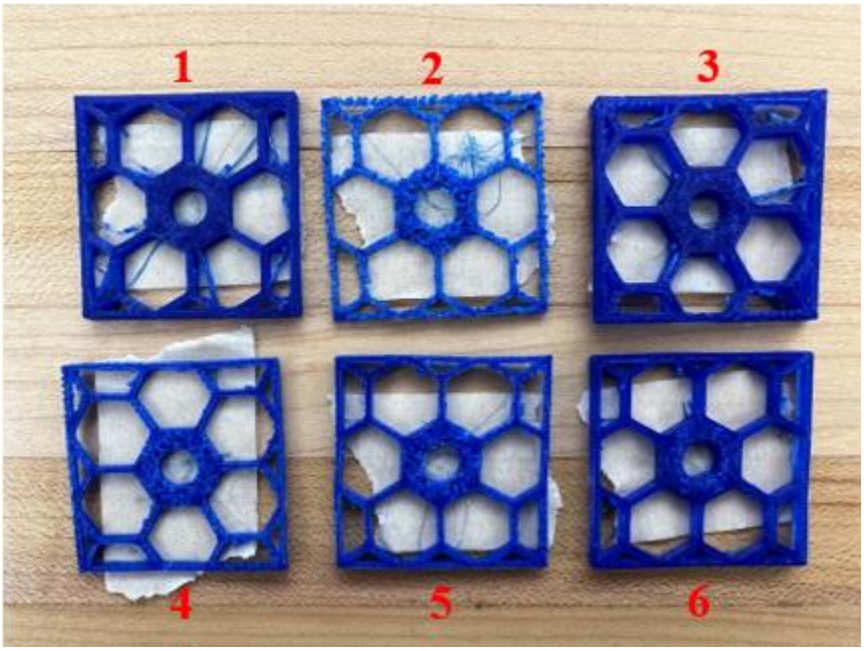

Figure 4.3. Printed test geometries to determine optimum printing parameters for NinjaFlex.

The quality of the sixth sample was satisfactory with minimal stringing, good layer adhesion, and nearly uniform density throughout the print. The printing parameters from the sixth sample were used to print all the hexagonal shock samples and the key ones are shown in Table 4.1.

Table 4.1. NinjaFlex TPU Printing Parameters

Layer Height	$0.1\ mm$	Wall Speed	$15\ mm/s$
Wall Line Count	4	Travel Speed	$200\ mm/s$
Infill Density	100 %	Initial Layer Speed	$15\ mm/s$
Printing Temperature	$240\ °C$	Initial Layer Travel Speed	$200\ mm/s$
Build Plate Temperature	$50\ °C$	Skirt/Brim Speed	$15\ mm/s$
Diameter	$1.75\ mm$	Print Acceleration	$1000\ mm/s^2$
Flow	120%	Travel Acceleration	$5000\ mm/s^2$
Enable Retraction	Yes	Combing Mode	All
Retraction Distance	$1\ mm$	Enable Print Cooling	Yes
Retraction Speed	$30\ mm/s$	Generate Support	No
Print Speed	$30\ mm/s$	Build Plate Adhesion Type	$Skirt$
Infill Speed	$15\ mm/s$		

4.2.2. Stiffness and Damping Testing Without Damping Material

12 TPU designs were tested with empty cells (no foam or Sorbothane) and with varying wall thicknesses and cell sizes. The stiffness and damping coefficients of each design are shown below in Table 4.2.

Table 4.2. Stiffness and damping coefficients for all 12 samples as computed by the least-squares regression on the force and displacement data.

Sample Name	Stiffness $\left(\frac{N}{m}\right)$	Damping $\left(\frac{Ns}{m}\right)$	Impact Velocity $\left(\frac{m}{s}\right)$
Honey10_40	22967	34	2.48
Honey10_60	36391	43	2.34
Honey10_80	45235	49	2.50
Honey17_40	12874	20	2.45
Honey17_60	15292	26	2.47
Honey17_80	18474	33	2.52
Honey30_40	5219	8	2.55
Honey30_60	10052	14	2.48
Honey30_80	14653	24	2.55
Honey40_40	5027	3	2.45
Honey40_60	8364	11	2.54
Honey40_80	12557	17	2.47

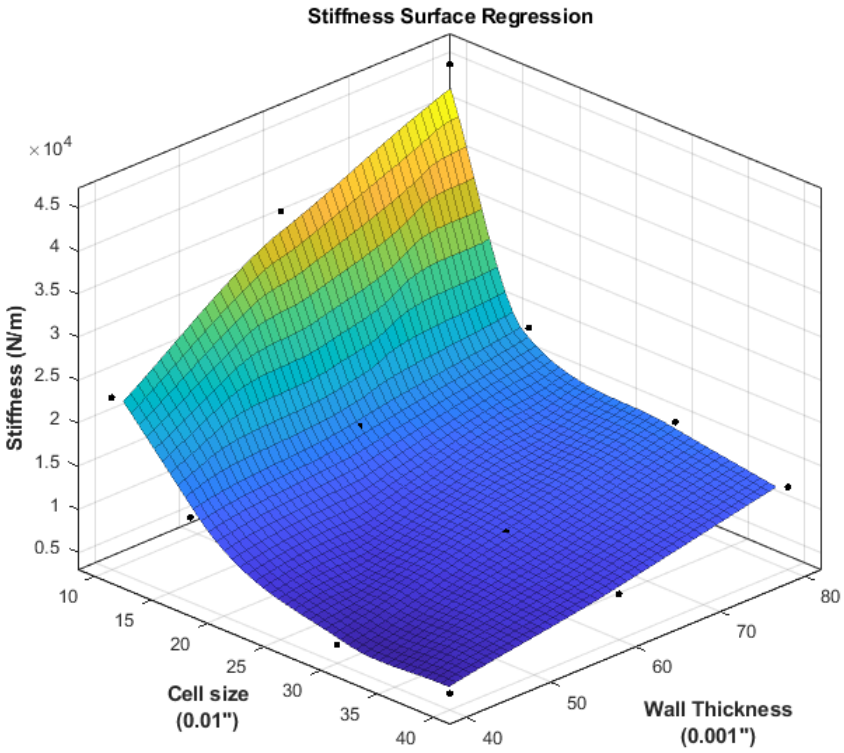

Figure 4.4. Interpolant cubic surface regression of stiffness coefficients

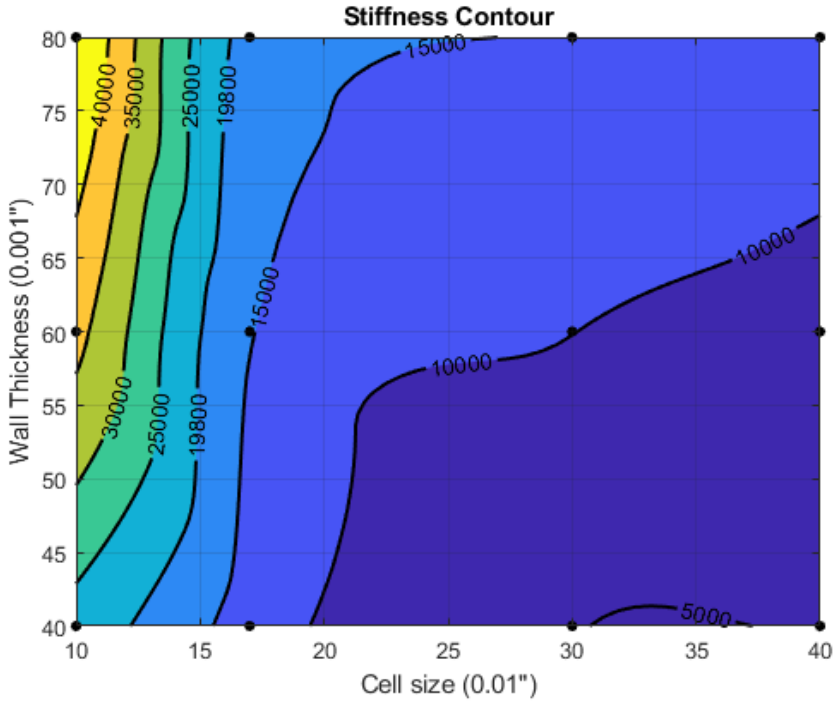

Figure 4.5. Stiffness contour plot showing the target stiffness level line of 19800 N/m

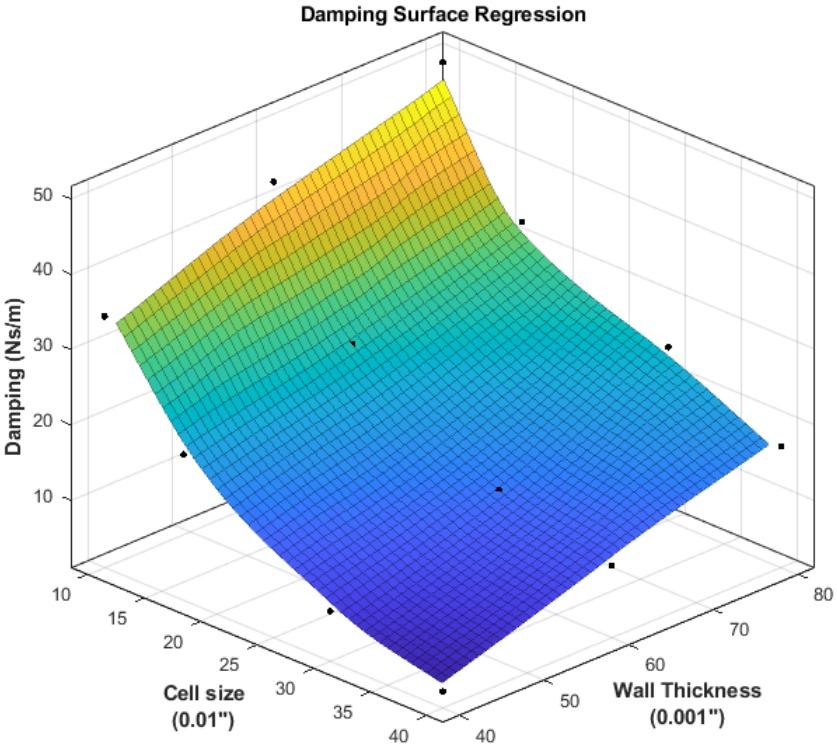

Figure 4.6. Interpolant cubic surface regression of damping coefficients

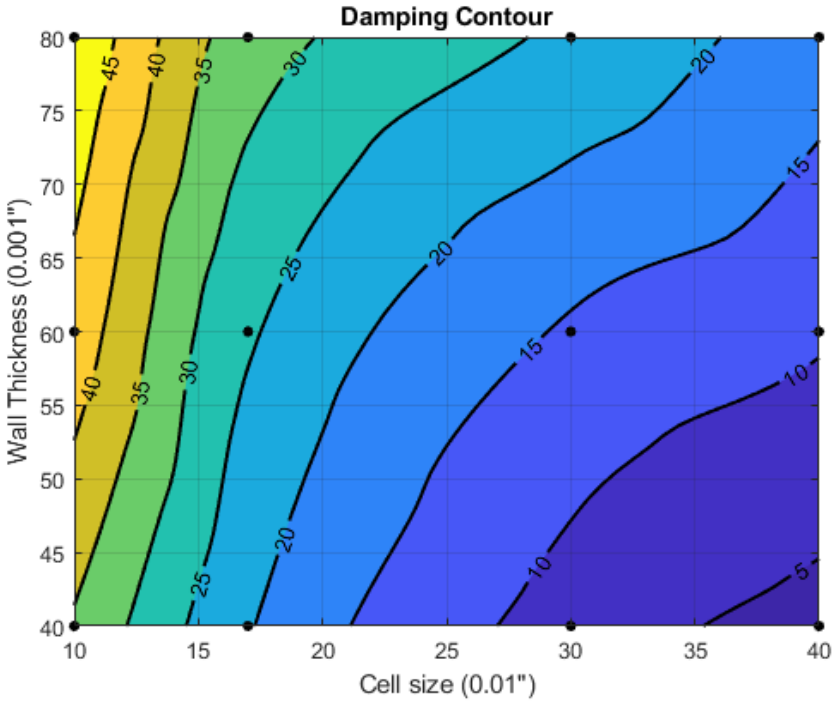

Figure 4.7. Damping contour plot. The target damping coefficient of $580\frac{Ns}{m}$ is a full order of magnitude larger than the largest computed damping coefficient

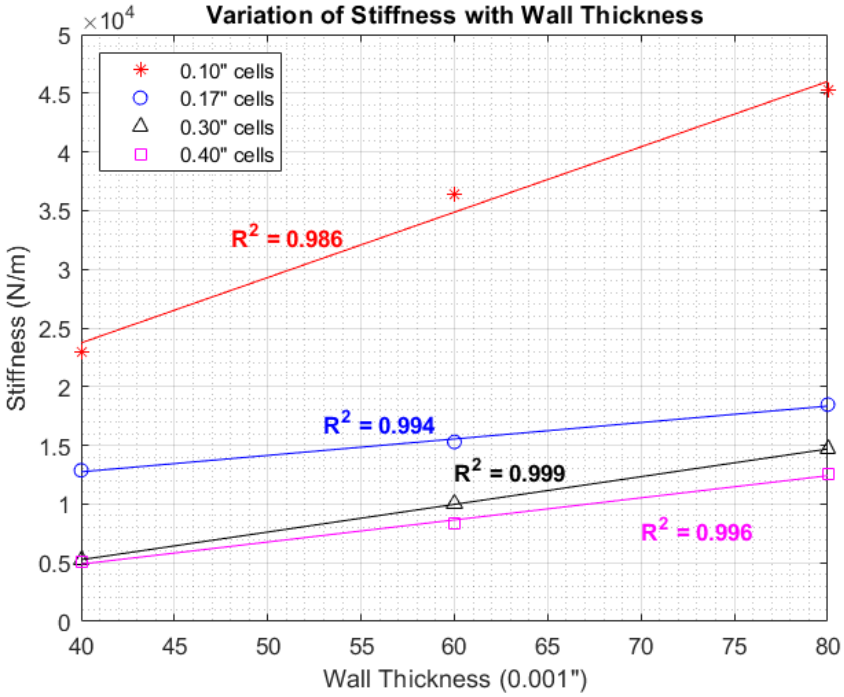

0.10”	$S = 557W + 1462$
0.17”	$S = 140W + 7146$
0.30”	$S = 236W - 4176$
0.40”	$S = 188W - 2646$

Figure 4.8. Linear relationship of stiffness and wall thickness

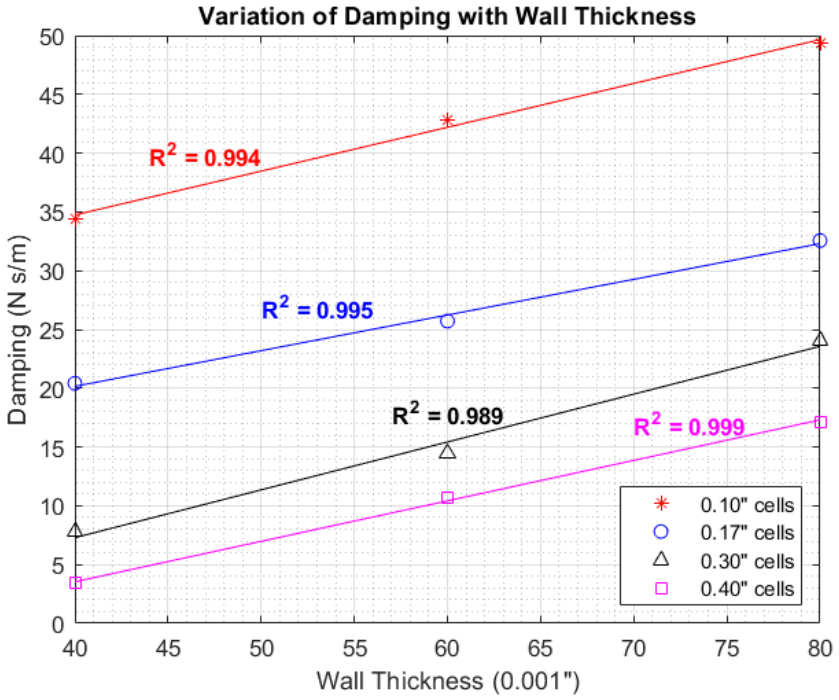

0.10”	$D = 0.37W + 19.82$
0.17”	$D = 0.30W + 8.02$
0.30”	$D = 0.41W - 8.99$
0.40”	$D = 0.34W - 10.24$

Figure 4.9. Linear relationship of damping and wall thickness

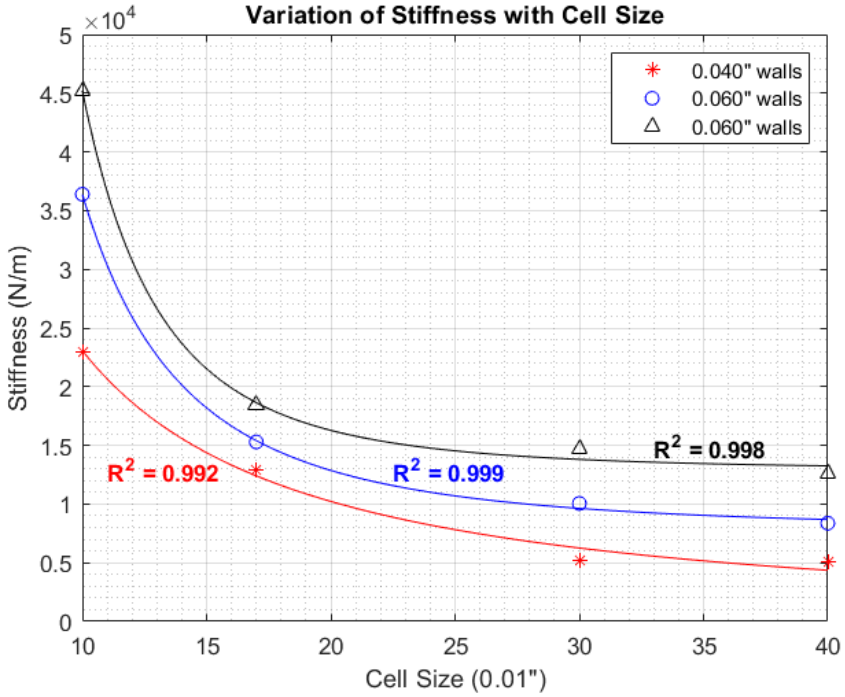

0.040”	$S = 3.19e5C^{-1.31} - 566$
0.060”	$S = 8.88e6C^{-2.49} + 7780$
0.080”	$S = 5.86e7C^{-3.26} + 12900$

Figure 4.10. Power law relationship between stiffness and cell size

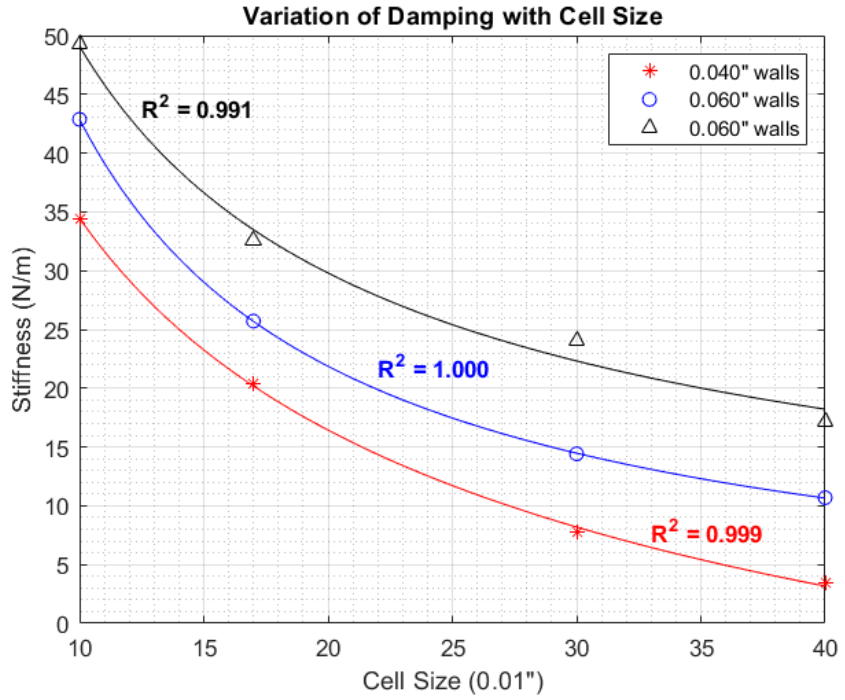

0.040”	$D = 189C^{-0.442} - 33.84$
0.060”	$D = 362.7C^{0.906} - 2.18$
0.080”	$D = 263.3C^{-0.737} + 0.854$

Figure 4.11. Power law relationship between damping and cell size

4.2.3. Target Samples

To achieve the target stiffness of 19800 $\frac{N}{m}$, suitable combinations of wall thickness and cell size were read from Figure 4.5. A cell size of 0.15" and two wall thicknesses were chosen: 0.050" and 0.060". Two new samples shown below in Figure 4.12 were designed with these dimensions and then printed and tested. Note that these were the only samples printed from a new spool of filament. These will be referred to as "target samples."

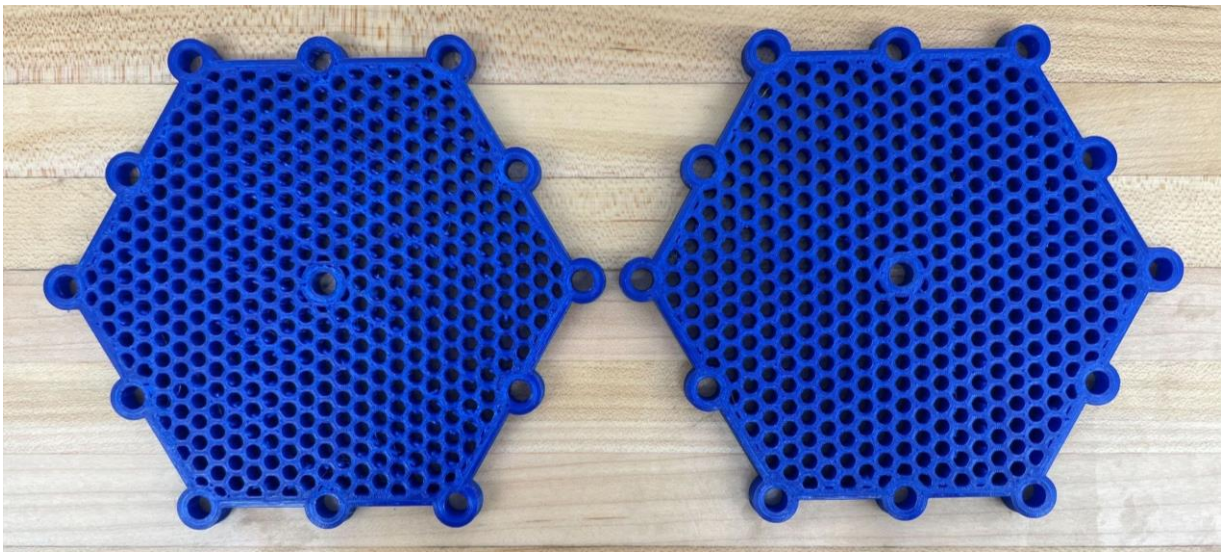

Figure 4.12. Target samples. Honey15_50 (left), Honey 15_60 (right)

Table 4.3. Stiffness and damping of target samples

Sample Name	Stiffness $\left(\frac{N}{m}\right)$	Damping $\left(\frac{Ns}{m}\right)$	Impact Velocity $\left(\frac{m}{s}\right)$
Honey15_50	23000 (19800/+16.6%)	31 (27/+14.8%)	2.34
Honey15_60	23667 (19800/+19.5%)	34 (30/+13.3%)	2.46

* Format: Sample Value (Contour Plot Prediction/Percent Error)

It was predicted that the large discrepancy between the predicted values and the actual values was due to differing material properties of the new spool. To investigate these differences, the Honey40_60 geometry was reprinted in the new material and both the old and the new samples were retested. The results shown below in Table 4.4 indicate that the new spool is 12% stiffer than the old spool.

Table 4.4. Comparing mechanical properties of Honey40_60 samples printed with old filament and new filament. The 95% confidence interval is shown for an indication of statistical significance.

Material	Stiffness $\left(\frac{N}{m}\right)$	Damping $\left(\frac{N\,s}{m}\right)$
Original spool	8099 ± 173	12.0 ± 3.7
New spool	9093 ± 159	14.1 ± 3.1

The stiffness of the target samples was adjusted to compensate for the change in material properties. The confidence intervals of the damping coefficients overlap, so the difference between these values is not statistically significant, and therefore, no adjustment can be made to the damping coefficients. The stiffness values were decreased by 12% and the new percent error was computed from this value. Table 4.5 below shows the adjusted mechanical properties of the target samples.

Table 4.5. Adjusted mechanical properties of the target samples.

Sample Name	Stiffness $\left(\frac{N}{m}\right)$	Damping $\left(\frac{Ns}{m}\right)$
Honey15_50	20240 (19800/+2.2%)	31 (27/+14.8%)
Honey15_60	20827 (19800/+5.2%)	34 (30/+13.3%)

* Format: Adjusted Sample Value (Contour Plot Prediction/Percent Error)

4.2.4. Stiffness and Damping Testing with Flex-Foam iT!

The honey40_40 design was filled with foam and retested to evaluate the damping capabilities of Flex Foam-iT!. Figure 4.13 below shows the force and displacement response comparison.

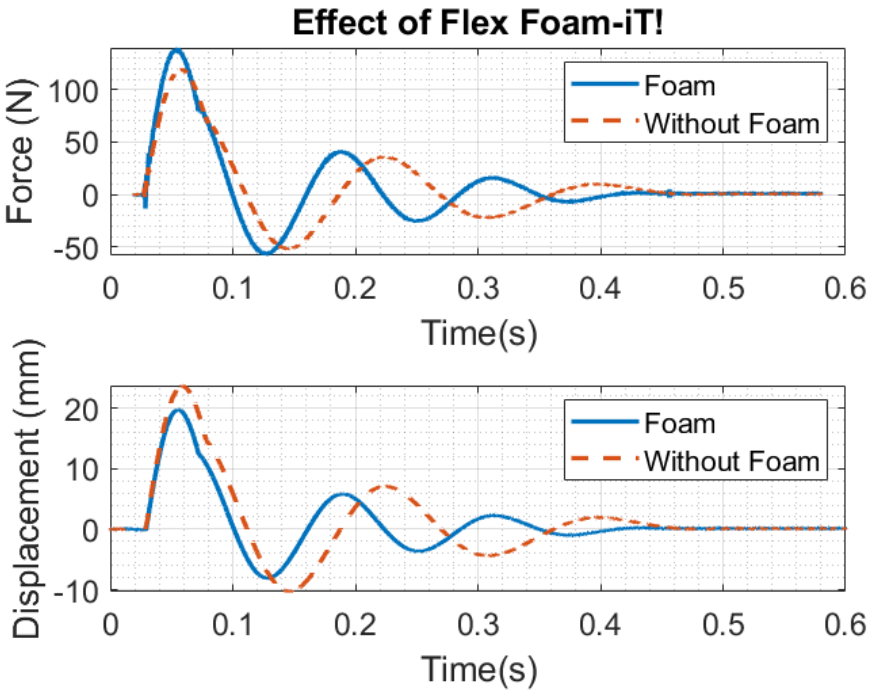

Figure 4.13. Comparison of honey40_40 shock design with foam and without foam

The stiffness and damping coefficients were computed with and without foam. These values are compared in Table 4.6 below.

Table 4.6. Effect of foam on stiffness and damping coefficients for honey40_40 sample

	Stiffness	Damping
Without Foam	$4996.8\frac{N}{m}$	$6.0\frac{Ns}{m}$
With Foam	$7038.6\frac{N}{m}$	$9.0\frac{Ns}{m}$
Percent Change	40.8 %	50 %

4.2.5. Stiffness and Damping Testing with Solid Sorbothane Shock

The solid Sorbothane sample that was waterjet out of sheet material (see Figure 3.5) was tested on the same impact testing machine but at a lower velocity of about 1 m/s to avoid maxing out the LVDT. The modeled fit is shown below in Figure 4.14. The stiffness coefficient was computed to be 481.3 $\frac{N}{m}$ and the damping coefficient was 11.59 $\frac{Ns}{m}$.

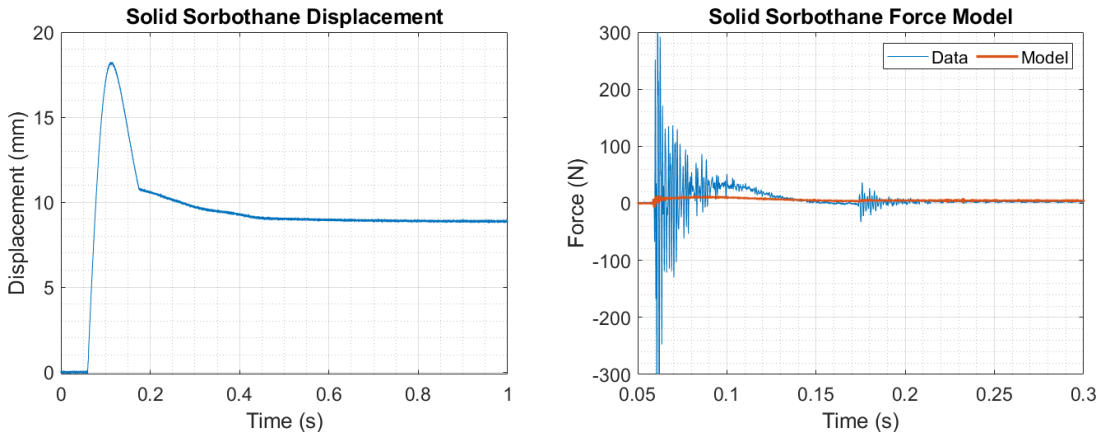

Figure 4.14. Solid Sorbothane hexagonal shock response to 1 m/s impact: Displacement (left), Force response fit with parallel mass spring damper model (right)

4.3. Discussion

4.3.1. Stiffness and Damping Testing without Damping Material

The stiffness, as shown in Figure 4.4, has a direct and monotonic relationship with wall thickness while exhibiting an inverse monotonic relationship with cell size. That is larger walls and smaller cells will increase the stiffness of the sample. This is expected because as the wall thickness increases and the cell size decreases, the sample geometry approaches that of a solid sample, which intuitively should have the largest stiffness. Over the short range tested, the stiffness appears to be nearly linear with wall thickness as shown in Figure 4.8. The stiffness has a power law relationship with the cell size, increasing rapidly as the cell size approaches small values as shown in Figure 4.10. More data points should be obtained in the range from 0” to 0.10” cell size to confirm this trend. Samples were periodically retested to ensure the consistency of the machine output and to test for any stiffness variance that may occur over time. No such trends were detected, and the machine remained consistent for the entire testing period.

4.3.2. Target Samples

The target stiffness coefficient of $19800\,\frac{N}{m}$ is within the range of the stiffnesses for the samples tested. The surface regression and contour plots can be used to interpolate and estimate a

combination of cell size and wall thickness that will produce the desired stiffness. The contour plot in Figure 4.5 shows that for the target level curve of 19800, the correct cell size is the most important factor in achieving the desired stiffness. The target level curve is nearly vertical over a wide range of wall thicknesses indicating that many wall thicknesses are possibilities as long as the cell size is chosen correctly. When choosing the combination of dimensions, the wall thickness was desired to be greater than or equal to 0.060" because the Dremel 3D45 printer struggles printing thin-walled TPU structures (due to the leaking of TPU and the inability to limit travel paths within the thin walls, aka "combing". See section 3.4 for further detail on printability). In addition, small cell sizes require a high X-Y print resolution to capture the small walls and sharp angles of each hexagon cell. Because of this, the Dremel 3D45 struggled printing the 0.10" cell size geometries, so the chosen combination should have a cell size larger than 0.10".

The testing of both target samples yielded stiffnesses of approximately 23000 $\frac{N}{m}$ which is 16% higher than the predicted stiffness of 19800 $\frac{N}{m}$. This error is unexpected given the high correlation coefficients of Figure 4.8 and Figure 4.10. The trend of stiffness with cell size and wall thickness was precisely captured, but both target samples seem to be outliers compared to the data set. Other samples were retested and produced similar stiffness and damping values as before indicating that the machine was not the cause of the discrepancy. Both samples do exhibit similar stiffnesses to each other as predicted by the surface contour. Since the trend relative to each other is accurate, this implies that it is not an error in the testing but some true difference in the mechanical properties of the shock absorber. The cause was predicted to be the filament itself. The original 12 samples were printed from the same roll of NinjaFlex filament. This spool

ran out and the target samples were printed from a new spool. Even though it was the same type of filament, there is a history of inconsistency of filament properties from spool to spool [14].

The suspicion of differing material properties between the two spools was confirmed by reprinting an original geometry (Honey40_60) with the new filament, testing both Honey40_60 samples (new material and old material), and comparing the results. It was found that the new material was 12% stiffer than the old material. To compensate for the change in material properties, the measured stiffness of the target samples was decreased by 12% to make an adjusted stiffness and an adjusted percent error shown in Table 4.5. The Honey15_50 sample has an adjusted percent error of only 2.2% and the Honey15_60 sample has an adjusted percent error of 5.2%, both of which are considered acceptable accuracy.

The target damping value of 580 $\frac{Ns}{m}$ is a full order of magnitude larger than the largest computed damping coefficient of 49 $\frac{Ns}{m}$. This indicates that the bare TPU samples are well below the required amount of damping for the helmet application and would benefit from the addition of a highly damped material. This low damping of the bare TPU was expected and is required if decoupling of the stiffness and damping in a multi-material shock absorber is to be achieved.

4.3.3. Stiffness and Damping Testing with Flex-Foam iT!

While the Flex Foam-iT material provided a 50% increase in damping for the honey40_40 sample, the magnitude of the damping is still an order of magnitude below the target. The system remained an underdamped system with the foam only slightly decreasing the magnitude of the oscillations while the response time was nearly unaffected. An ideal damping material would create an over-damped system which eliminates the oscillations and dissipates the impact energy over a longer time. The foam also increased the stiffness by over 2000 N/m which is a 40% increase and a full 10% of the total target stiffness. It was deemed that Flex

Foam-iT! added too much stiffness and not enough damping, and this material was dismissed from consideration.

4.3.4. Stiffness and Damping Testing with Solid Sorbothane Shock

The Sorbothane material did not exhibit any oscillations which indicates an over-damped system. The sample, however, lacked the necessary stiffness to return the material to its original shape following impact. The 481 $\frac{N}{m}$ stiffness coefficient is a full order of magnitude lower than the least stiff TPU sample. While the observations are consistent with those of a highly damped material, the computed damping coefficient of only 11.59 $\frac{Ns}{m}$ does not agree. The computed stiffness and damping coefficients should not be trusted because the force model shown in Figure 4.14 clearly shows that the model does not accurately capture the dynamics of the system. This material likely does not behave like the parallel spring-damper system that was assumed. To improve accuracy and reliability of the results, the data should be fit with a new type of model that more accurately captures its behavior or a new method should be employed to compute the stiffness and damping coefficients.

CHAPTER 5. CONCLUSIONS

A new helmet design has been proposed that addresses both translational and rotational accelerations of a collision via the addition of a second helmet shell. A 3D lumped parameter model was used to simulate the response of a helmet to a full helmet test protocol and was optimized to determine a combination of stiffness and damping coefficients that would achieve the target HPS of 0.7. It was shown through modeling and simulation that allowing relative rotation between the helmet and the head can reduce the Helmet Performance Score (HPS) by 48% or more.

The implementation of these modeled results required achieving the optimal rotational stiffness and damping properties using a suitable combination of material and geometry. Multi-material hexagonal shock absorbers were created in an attempt to decouple and independently tune the stiffness and damping when designing the shock absorber. The shock absorber design consists of a 3D printed honeycomb backbone made of TPU and a highly damped material to fill the voids. A sample was designed within 2.2% of the target stiffness; however, no material tested was able to provide enough damping to achieve the optimal damping coefficient. The damping of all designs remained an order of magnitude lower than the target value.

Future work should be aimed at solving the damping problem. Sorbothane shows promise of high damping capabilities; however, the current material model of a parallel spring-damper is not a good fit and failed to produce an accurate least-squares regression on the test data. This led to inaccurate quantification of the stiffness and damping and potentially improper assessment of its damping potential. New material models that accurately characterize Sorbothane's viscoelastic behavior should be investigated. Another way to potentially increase the damping of the shock absorber is to engage more of the material in the deformation by changing the pin

pattern. The current mounting method has pins around the perimeter of the sample and fixed only to the bottom plate. The only deformation is localized around the center pin. This local deformation only engages a small portion of the material. If the pin pattern on the test fixture is changed so that the perimeter pins are alternated between the top and bottom plates, the relative motion of the plates (or helmet shells in the rotational sense) will deform the majority of the material which should increase the damping. If a new pin pattern does not sufficiently improve the damping, new materials and geometries may need to be explored. It may be necessary to revisit other designs such as a shock absorber with hollow, deformable bubbles connected via channels. This design employs the viscous damping of the fluid traveling between cells through the narrow channel orifice. If filled with a sufficiently viscous material, it may have the potential to generate the necessary amount of damping.

This research has demonstrated that the next generation of football helmet designs need to reduce the rotational accelerations of the head during collisions to significantly reduce brain strain and protect athletes against TBIs.

APPENDIX A. SIMSCAPE MODELS AND RESPONSE OPTIMIZER

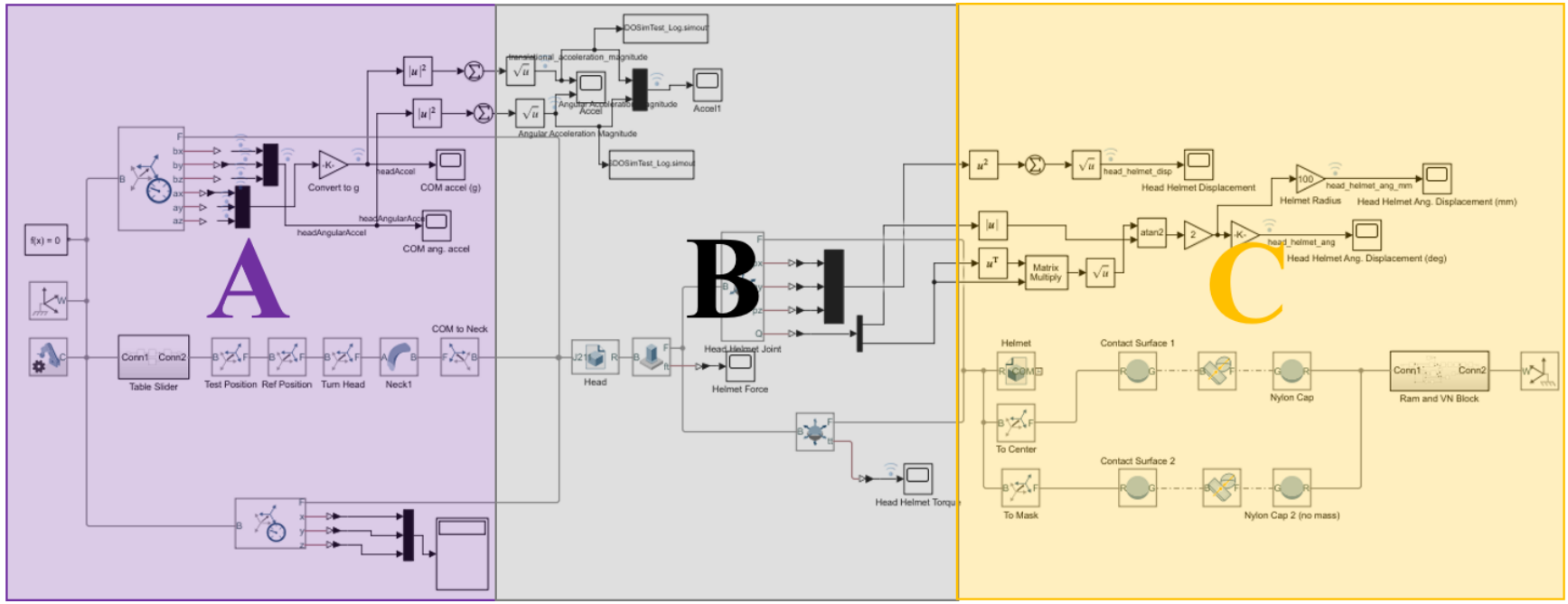

Figure A.1. Sectioned 6 DOF, 3D lumped parameter model to simulate the NFL Helmet Challenge test protocol. See subsequent figures for close-ups of each section.

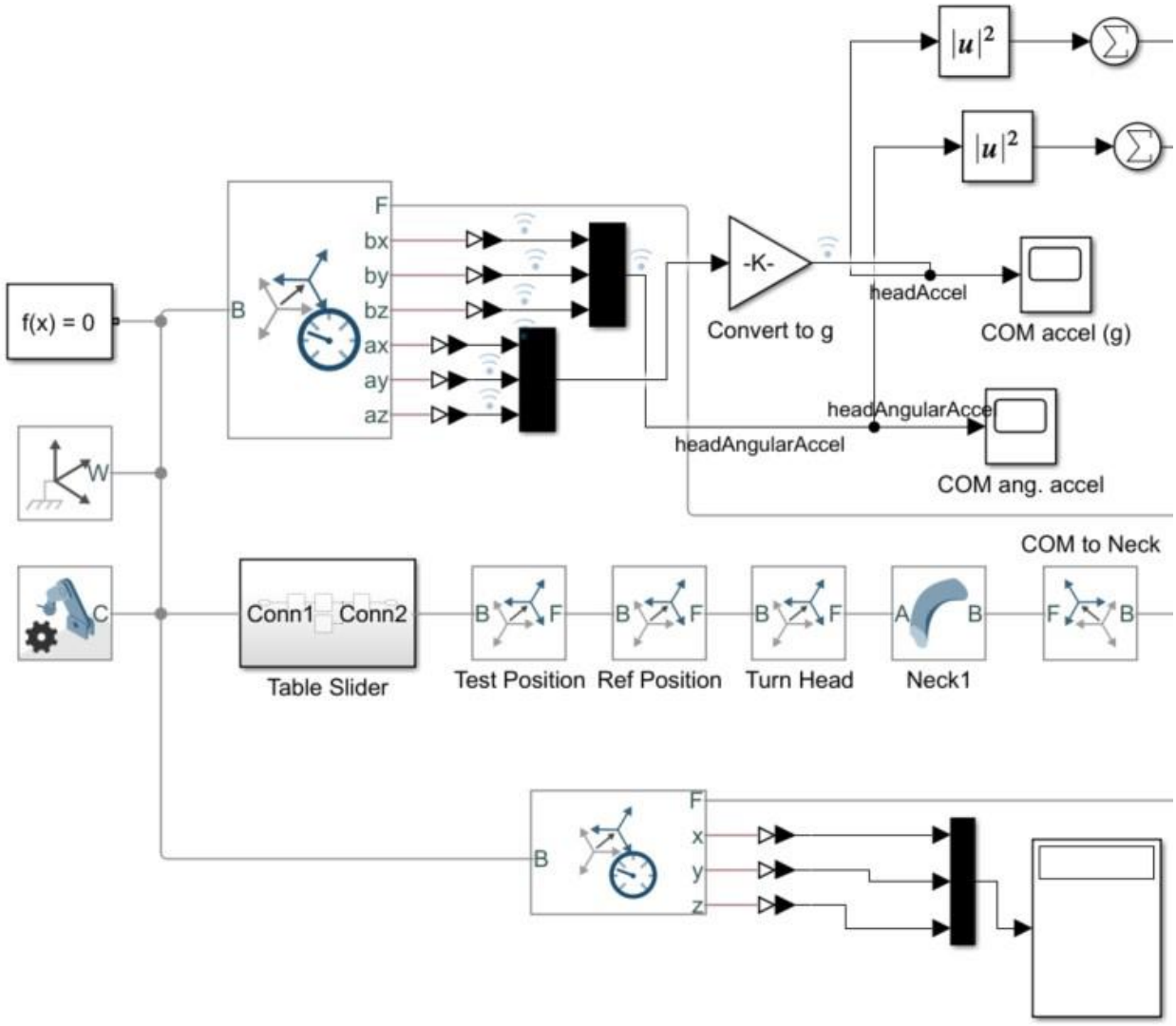

Figure A.2. Section A of the 3D lumped parameter Simscape model

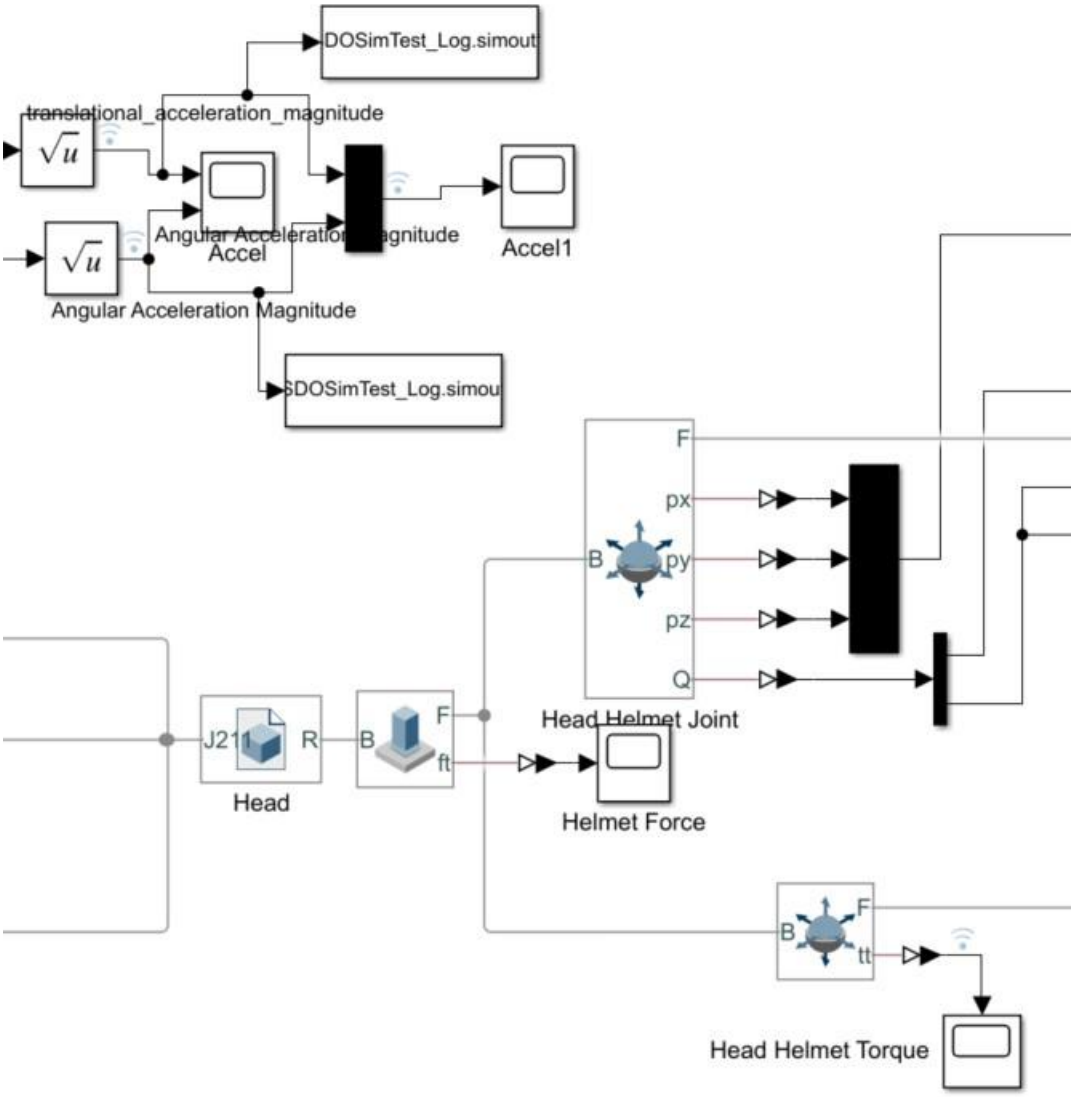

Figure A.3. Section B of the 3D lumped parameter Simscape model

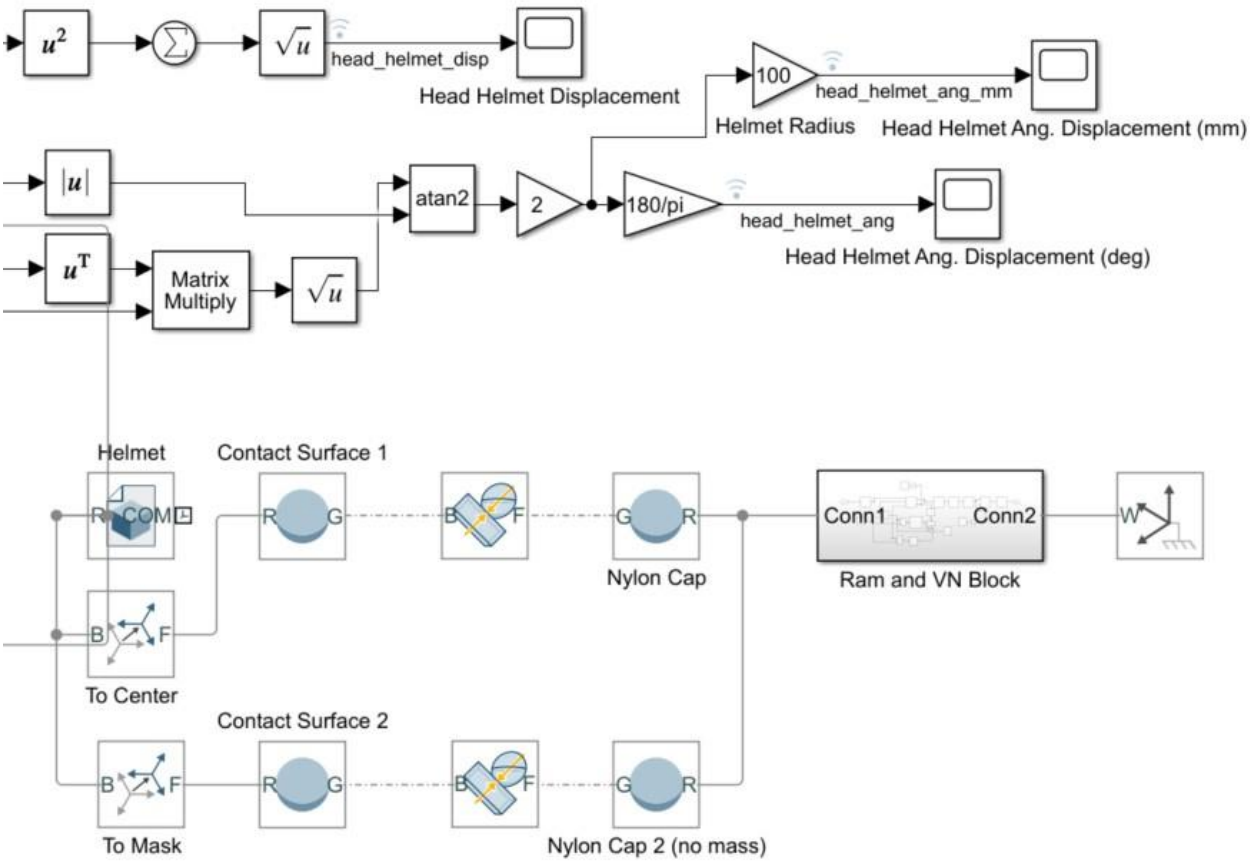

Figure A.4. Section C of the 3D lumper parameter Simscape model

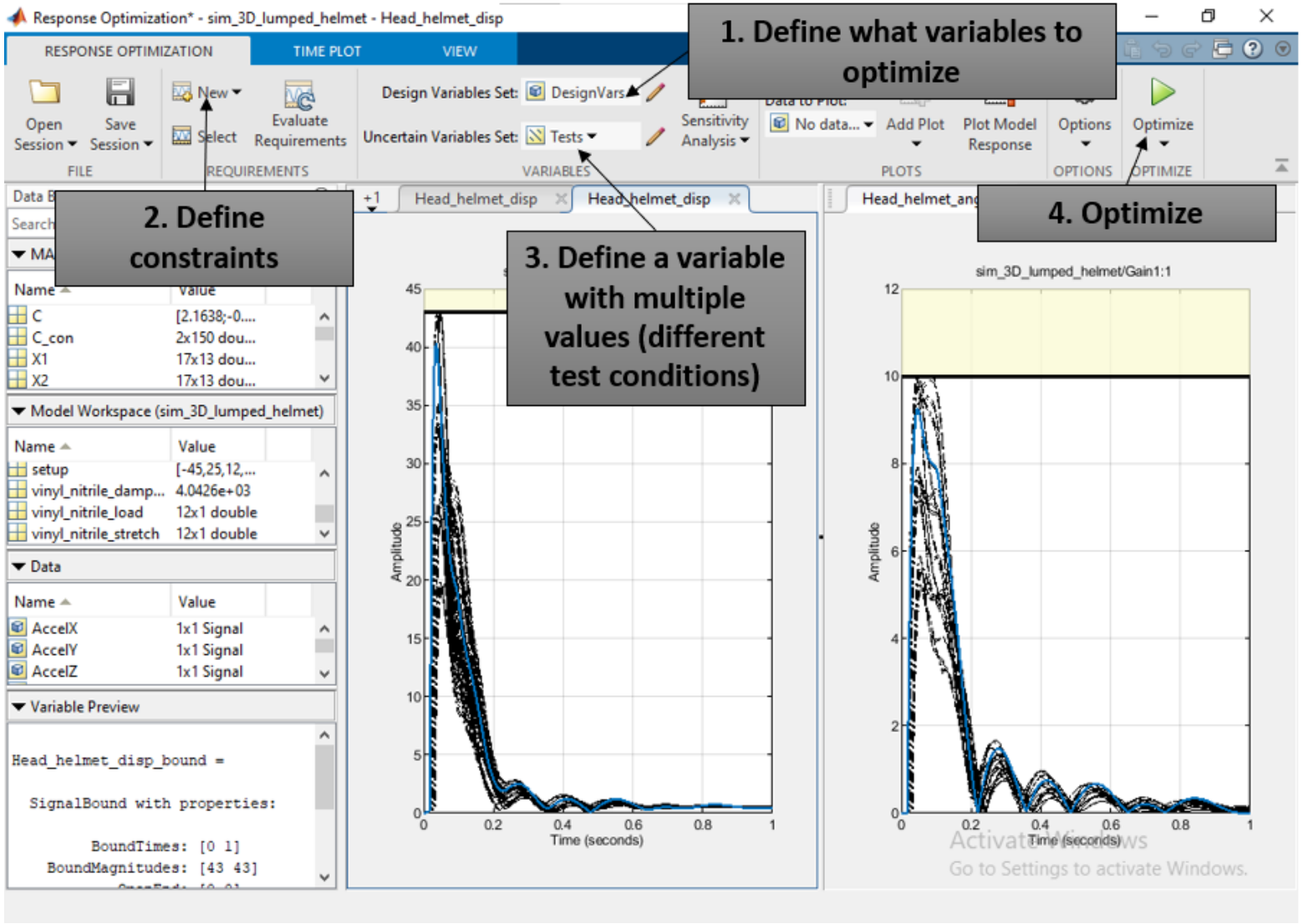

Figure A.5. Simulink Response Optimizer GUI with steps

APPENDIX B. MATLAB CODES

HIC.m

```
function Y = HIC_linear(X)
% ------------------------------------------------------------------------
% Version: 1.0 (Released: March 2019)
% ------------------------------------------------------------------------
% This script calculates the Head Injury Criterion (HIC): Versace, J. A
% Review of the Severity Index. Warrendale: SAE International, 1971.
% ------------------------------------------------------------------------
% Administrative contact: Lee F. Gabler (lgabler@biocorellc.com)
% ------------------------------------------------------------------------
% Use of this software is subject to the terms of the software agreement
% at http://biocorellc.com/software/.
% ------------------------------------------------------------------------
% Input variable:
% X: Timed head kinematics (nx4), where n is the # of time points.
%    Column 1: Time (s)
%    Column 2: linear acceleration (g)
%    Data entered must be measured with respect to the local head
%    coordinate system defined by SAE J211. Do not enter column headers.
%
% Output variable:
% Y: Data structure containing HIC metric output.
% ------------------------------------------------------------------------
%
% setup
n = length(X);
t = X(:,1);   % time (s)
a = X(:,2); % linear acceleration (g)
%
% calculate HIC
hic = 0;
hic_t = zeros(n,1);
V = zeros(n,1);
A = sum(a.*a,2).^(0.5);% resultant linear acceleration (g)
for i = 2:n
    V(i) = V(i-1)+0.5*(A(i)+A(i-1))*(t(i)-t(i-1));% velocity (g*s)
    for j = i-1:-1:1
        dt = t(i)-t(j);
        if dt<0.015% 15 ms limit
            h = dt*((V(i)-V(j))/dt)^2.5;
            if h>hic
                hic = h;
                hic_t(i) = hic;
                tmin = t(j);
                tmax = t(i);
            end
        end
    end
    if hic_t(i)<hic_t(i-1)
        hic_t(i) = hic_t(i-1);
    end
end
%
```

```
% output
Y.t = t;          % time (s)
Y.hic_t1 = tmin; % HIC t1 (s)
Y.hic_t2 = tmax; % HIC t2 (s)
Y.hic = hic;      % HIC metric
Y.hic_t = hic_t; % HIC metric over time (nx1)
End
```

DAMAGE.m

```
function Y = DAMAGE(X)
% ------------------------------------------------------------------------
% Version: 1.0 (Released: March 2019)
% ------------------------------------------------------------------------
% This script calculates the Diffuse Axonal, Multi-Axis, General Evaluation
% (DAMAGE) metric: Gabler, L.F., Crandall, J.R. & Panzer, M.B. Ann Biomed
% Eng, 2018. https://doi.org/10.1007/s10439-018-02179-9.
% ------------------------------------------------------------------------
% Administrative contact: Lee F. Gabler (lgabler@biocorellc.com)
% Research contact: Matthew B. Panzer (panzer@virginia.edu)
% ------------------------------------------------------------------------
% Use of this software is subject to the terms of the software agreement
% at http://biocorellc.com/software/.
% ------------------------------------------------------------------------
% Input variable:
% X: Timed head kinematics (nx4), where n is the # of time points.
%    Column 1: Time (s)
%    Column 2: X angular acceleration (rad/s/s)
%    Column 3: Y angular acceleration (rad/s/s)
%    Column 4: Z angular acceleration (rad/s/s)
%    Data entered must be measured with respect to the local head
%    coordinate system defined by SAE J211. Do not enter column headers.
%
% Output variable:
% Y: Data structure containing DAMAGE metric output.
% ------------------------------------------------------------------------
%
% setup
n = length(X);
t = X(:,1);     % time (s)
alp = X(:,2:4); % angular acceleration (rad/s/s)
%
% calculate DAMAGE
B = 2.9903;                                    % (1/m) scale factor
F = [alp(:,1:2),-alp(:,3)];                    % excitation
dmg_i = B*rk4ode(n,t,F);                       % components of DAMAGE
dmg_t = cummax(sum(dmg_i.*dmg_i,2).^(0.5)); % DAMAGE over time
[dmg,~] = max(dmg_t);                          % DAMAGE metric
%
% output
Y.t = t;            % time (s)
Y.damage = dmg;     % DAMAGE metric
Y.damage_i = dmg_i; % DAMAGE components (nx3)
Y.damage_t = dmg_t; % DAMAGE metric over time (nx1)
end
```

```
function x = rk4ode(n,t,F)
% Solve for system displacements of the DAMAGE multibody model using
% Runge-Kutta 4th order method (RK4).
%
% multibody parameters
m = eye(3);                    % mass (kg)
kxx = 32142; kyy = 23493; kzz = 16935; kxy = 0; kyz = 0; kxz = 1636.3;
k = [kxx+kxy+kxz,-kxy,-kxz;  % stiffness matrix (N/m)
     -kxy,kxy+kyy+kyz,-kyz;
     -kxz,-kyz,kxz+kyz+kzz];
a1 = 5.9148*10^-3;             % damping constant (s)
c = a1*k;                      % proportional damping (Ns/m)
%
% RK4 method
x = zeros(n,3);   % displacements
dx = zeros(n,3);  % velocities
d2x = zeros(n,3); % accelerations
for i = 2:n
    h = t(i)-t(i-1); % time step
    k1x = dx(i-1,:);
    k1v = f(x(i-1,:),dx(i-1,:),F(i-1,:),m,c,k);
    k2x = dx(i-1,:)+k1v*(0.5*h);
    k2v = f(x(i-1,:)+k1x*(0.5*h),dx(i-1,:)+k1v*(0.5*h),0.5*(F(i-
1,:)+F(i,:)),m,c,k);
    k3x = dx(i-1,:)+k2v*(0.5*h);
    k3v = f(x(i-1,:)+k2x*(0.5*h),dx(i-1,:)+k2v*(0.5*h),0.5*(F(i-
1,:)+F(i,:)),m,c,k);
    k4x = dx(i-1,:)+k3v*h;
    k4v = f(x(i-1,:)+k3x*h,dx(i-1,:)+k3v*h,F(i,:),m,c,k);
    kx = (k1x+2*k2x+2*k3x+k4x)/6;
    kv = (k1v+2*k2v+2*k3v+k4v)/6;
    d2x(i,:) = kv;
    dx(i,:) = dx(i-1,:)+kv*h;
    x(i,:) = x(i-1,:)+kx*h;
end
end

function d2x = f(x,dx,F,m,c,k)
% Differential equations for DAMAGE multibody model
d2x(1,1) = (F(1)-c(1,1)*dx(1)-c(1,2)*dx(2)-c(1,3)*dx(3)-k(1,1)*x(1)-
k(1,2)*x(2)-k(1,3)*x(3))/m(1,1);
d2x(1,2) = (F(2)-c(2,1)*dx(1)-c(2,2)*dx(2)-c(2,3)*dx(3)-k(2,1)*x(1)-
k(2,2)*x(2)-k(2,3)*x(3))/m(2,2);
d2x(1,3) = (F(3)-c(3,1)*dx(1)-c(3,2)*dx(2)-c(3,3)*dx(3)-k(3,1)*x(1)-
k(3,2)*x(2)-k(3,3)*x(3))/m(3,3);
end
```

HARM.m

```
function Y = HARM(X)
% -------------------------------------------------------------------------
% Version: 1.0 (Released: March 2019)
% Required matlab functions: HIC.m and DAMAGE.m (v1.0)
% -------------------------------------------------------------------------
% This script calculates the Head Acceleration Response Metric (HARM) and
% associated metrics: Head Injury Criterion (HIC) and Diffuse Axonal,
```

```
% Multi-Axis, General Evaluation (DAMAGE) metric:
%
% HIC: Versace, J. A Review of the Severity Index. Warrendale: SAE
% International, 1971.
%
% DAMAGE: Gabler, L.F., Crandall, J.R. & Panzer, M.B. Ann Biomed Eng, 2018.
% https://doi.org/10.1007/s10439-018-02179-9.
% ------------------------------------------------------------------------
% Administrative contact: Lee F. Gabler (lgabler@biocorellc.com)
% Research contact (for DAMAGE): Matthew B. Panzer (panzer@virginia.edu)
% ------------------------------------------------------------------------
% Use of this software is subject to the terms of the software agreement
% at http://biocorellc.com/software/.
% ------------------------------------------------------------------------
% Input variable:
% X: Timed head kinematics (nx7), where n is the # of time points.
%    Column 1: Time (s)
%    Column 2: X CG linear acceleration (g)
%    Column 3: Y CG linear acceleration (g)
%    Column 4: Z CG linear acceleration (g)
%    Column 5: X angular acceleration (rad/s/s)
%    Column 6: Y angular acceleration (rad/s/s)
%    Column 7: Z angular acceleration (rad/s/s)
%    Data entered must be measured with respect to the local head
%    coordinate system defined by SAE J211. Do not enter column headers.
%
% Output variable:
% Y: Data structure containing HIC, DAMAGE, and HARM metric ouputs.
% ------------------------------------------------------------------------
%
% setup
t = X(:,1);     % time (s)
a = X(:,2:4);   % linear acceleration (g)
alp = X(:,5:7); % angular acceleration (rad/s/s)
%
% calculate HIC
H = HIC([t,a]);
%
% calculate DAMAGE
D = DAMAGE([t,alp]);
%
% calculate HARM
C1 = 14.81*10^-3;
C2 = 15.60;
harm_hic = C1*H.hic;
harm_dmg = C2*D.damage;
harm = harm_hic + harm_dmg;
harm_t = C1*H.hic_t + C2*D.damage_t;
%
% output
Y.t = t;                    % time (s)
Y.hic_t1 = H.hic_t1;        % HIC t1 (s)
Y.hic_t2 = H.hic_t2;        % HIC t2 (s)
Y.hic = H.hic;              % HIC metric
Y.hic_t = H.hic_t;          % HIC metric over time (nx1)
%
Y.damage = D.damage;        % DAMAGE metric
```

```
Y.damage_i = D.damage_i;  % DAMAGE components (nx3)
Y.damage_t = D.damage_t;  % DAMAGE metric over time (nx1)
%
Y.harm = harm;            % HARM metric
Y.harm_hic = harm_hic;    % HARM from HIC
Y.harm_damage = harm_dmg; % HARM from DAMAGE
Y.harm_t = harm_t;        % HARM metric over time (nx1)
end
```

HPS.m

```
function y = HPS(harm_scores)
%UNTITLED5 Summary of this function goes here
%   Detailed explanation goes here
load NFL_Helmet_Test_Protocol.mat weights

y = weights'*harm_scores;

end
```

optimization_surface_regression.m

```
 %% Optimiztion_surface_regression
%Code used to add new rows to the phi and y matrices
%phi=[8x6] matrix containing all combinations of constraint
%variables in the 2-variable quadratic equation

%phi=[1 x1' x2' x1x2' x1^2' x2^2'; 1 x1'' x2'' x1x2'' ...]

%% Create matrices from constraints and optimized HPS
x1=[25 18.75 18.75 31.25 31.25 25 16.16 25 33.84 33.84 33.84 40 40 32.5 45 30
43];  %Translational displacement constraint [mm]
x2=[5 7 3 3 7 7.83 5 2.17 5 7.83 8 7 5 9 5 11 10];   %Angular displacement
constraint [degrees]
y=[0.9248 0.9357 1.2633 0.9354 0.7594 0.8046 1.123 1.1388 0.8153 0.7117
0.7075 0.6811 0.7283 0.6991 0.6888 0.6756 0.6139];  %HPS (verify element 1)
Y=y';

% Y=y(1); %first row of Y matrix
phi=[1 x1(1) x2(1) x1(1)*x2(1) x1(1)^2 x2(1)^2];    %first row of phi matrix

%for loop to define each new row
for i=2:numel(x1)
% Y=[Y;y(i)];
phi=[phi;...
    1 x1(i) x2(i) x1(i)*x2(i) x1(i)^2 x2(i)^2];
end

C=phi\Y;    %solve for coefficients
residuals=phi*C-Y

%% Define anonymous function using coefficients
close all
clf;
```

```
[X1,X2]=meshgrid([10:2.5:40],[2:0.5:10]);
Z=C(1)+C(2).*X1+C(3).*X2+C(4).*X1.*X2+C(5).*X1.^2+C(6).*X2.^2;
s=surf(X1,X2,Z,'FaceAlpha',0.75,'EdgeColor',[0,0,0]);
xlabel('\Delta (mm)')
ylabel('\theta (deg)')
zlabel('Helmet Performance Score')
title('Optimization Surface - HPS')
view(135,30)
% set(gca,'XTickLabel',{' '})
% set(gca,'YTickLabel',{' '})
% set(gca,'ZTickLabel',{' '})
xh=get(gca,'XLabel')
pos=get(xh,'Position');
set(xh,'Position',pos.*[0.9,1.1,1])
yh=get(gca,'YLabel')
pos=get(yh,'Position')
set(yh,'Position',pos.*[1.15,0.8,1])
lighting gouraud
% shading interp
% light
camlight right

hold on
plot3(x1,x2,Y,'r*')

figure
[C_con,h]=contour(X1,X2,Z);
xlabel('\Delta_m (mm)','FontSize',18)
ylabel('\theta_m (deg)','FontSize',18)
clabel(C_con,h,'FontSize',18)
% set(gca,'XTickLabel',{' '})
% set(gca,'YTickLabel',{' '})
title('Contour of HPS','FontSize',18)
hold on
plot(x1(1:14),x2(1:14),'ro')
h.LineWidth=2;
%% Comments on Results
%min Z occurs at cell 61,10 (33mm,8deg)
%graph increases in the correct direction
%slope is steeper in the translational dirction indicating a stronger
%impact on the HPS (same trend previously observed)
%interesting that the min occurs at 33 and not at max translational
%displacement (this is likely due to extrapolation of the curve fit)
```

fit_model.m

```
%% This one is used when data is automatically written as .txt file
function [xmax,res,R2,b,k]=fit_model(folder, test_name)
clf;clc;
load LFP.mat
subplot(3,1,1);
dt = 1/50000; %inverse of sample rate
% Displacement data should be loaded in table TestDisp with columns
%  Time_Dev1_ai2
```

```
disp_file = [folder '\LVDT Test ' test_name '.txt'];
load_file = [folder '\Load Cell Test ' test_name '.txt'];
vel_file = [folder '\Velocity Test ' test_name '.txt'];
%load_file = '288-003, Test1, 3D printed black 4.16.2021 LoadCell.txt';

TestDisp = readtable(disp_file);
TestLoad = readtable(load_file);
TestVel = importdata(vel_file);



load_cell_scale = 199.43; %N/V

fit_begin = 1000;

Tab = TestDisp;
Tab.Disp = (Tab.Var2-mean(Tab.Var2(1:fit_begin)))/1.7443/100;    %1.7443 V/cm
(lab day 2/25/22)
plot(Tab.Var1, Tab.Disp);
ylabel('Displacement (m)')
subplot(3,1,2);

fit_end = length(Tab.Disp)-1000;

Vel = 1/dt*diff(Tab.Disp);
Vel = filtfilt(Num,Den,Vel);
plot(Tab.Var1(1:end-1), Vel);
ylabel('Velocity (m/s)')


F = TestLoad.Var2(1:end,:)*load_cell_scale;
F = F-mean(F(1:1000));
subplot(3,1,3);
plot(TestLoad.Var1,F);

% Some models might need to use
%  dF/dt as one of the factors
% dFdt = 1/dt*diff(F);
% dFdt = filtfilt(Num,Den,dFdt);



Phi = [Vel(fit_begin:fit_end), Tab.Disp(fit_begin:fit_end)];     %convert to
m/s and m respectively
Ffit = F(fit_begin:fit_end);
theta = Phi\Ffit;
Fhat = Phi*theta;
hold on;
plot(TestLoad.Var1(fit_begin:fit_end), Fhat,'r-','LineWidth',1);
ylabel('Force (N)')
legend('Data','Model')

           %N/mm
res = sqrt(1/(fit_end-fit_begin+1)*sum((Ffit - Fhat).^2))
```

```
SStot = sum((Ffit-mean(Ffit)).^2);  %(Sy)^2
SSres = sum((Fhat-Ffit).^2);        %(Sy/x)^2
R2 = 1-SSres/SStot %(error in the degrees of freedom here. They don't cancel
with standard deviation. Unless m=0)
b = theta(1)            %(N*s)/mm
k = theta(2)
V_imp=TestVel(5)
xmax=max(Tab.Disp)

end
```

createFit.m

This code is was generated by Matlab's Curve Fitting Toolbox and then customized. This program creates the stiffness and damping surface regressions and contour plots shown in Figure 4.4 through Figure 4.7.

```
function [fitresult, gof] = createFit(x1, x2, y)
%CREATEFIT(X1,X2,Y)
%  Create a fit.
%
%  Data for 'Stiffness' fit:
%      X Input : x1
%      Y Input : x2
%      Z Output: y
%  Output:
%      fitresult : a fit object representing the fit.
%      gof : structure with goodness-of fit info.
%
%  See also FIT, CFIT, SFIT.

%  Auto-generated by MATLAB on 10-Jun-2022 13:30:20


%% Fit: 'Stiffness'.
clc;close all;
x1=[10 10 10 17 17 17 30 30 30 40 40 40];  %Cell Size [0.01 in]
x2=[40 60 80 40 60 80 40 60 80 40 60 80];   %Wall thickness [0.001 in]
y=[22967 36391 45235 12874 15291 18474 5219 10052 14653 5027 8364 12557];
%Stiffness (verify element 1)
%
[xData, yData, zData] = prepareSurfaceData( x1, x2, y );

% Set up fittype and options.
ft = 'cubicinterp';

% Fit model to data.
[fitresult, gof] = fit( [xData, yData], zData, ft, 'Normalize', 'on' );

% Plot fit with data.
figure( 'Name', 'Stiffness' );
```

```
h = plot( fitresult, [xData, yData], zData);
% legend( h, 'Stiffness', 'y vs. x1, x2', 'Location', 'NorthEast',
'Interpreter', 'none' );
% Label axes
h(2).MarkerFaceColor=[0 0 0];
h(2).MarkerEdgeColor=[0 0 0];
h(2).MarkerSize=4;
xlabel( 'x1', 'Interpreter', 'none' );
ylabel( 'x2', 'Interpreter', 'none' );
zlabel( 'y', 'Interpreter', 'none' );
grid on
view( 45,30 );

% Make contour plot.
figure( 'Name', 'Stiffness' );
v=[4000,5000,10000,15000,19800,25000,30000,35000,40000];
h = plot( fitresult, [xData, yData], zData, 'Style', 'Contour' );
h(1).LevelList=v;
h(1).ShowText='on';
h(1).LineWidth=1.5;
h(2).Marker='o';
h(2).Color=[0 0 0];
h(2).MarkerFaceColor=[0 0 0];
h(2).MarkerEdgeColor=[0 0 0];
h(2).MarkerSize=4;
% Label axes
xlabel( 'x1', 'Interpreter', 'none' );
ylabel( 'x2', 'Interpreter', 'none' );
grid on
title('Stiffness Contour')
xlabel('Cell size
(0.01")','FontWeight','normal','horizontalAlignment','center')
ylabel('Wall Thickness
(0.001")','FontWeight','normal','horizontalAlignment','center')
%% Fit: 'Damping'.
clc;close all;
x1=[10 10 10 17 17 17 30 30 30 40 40 40];  %Cell Size [0.01 in]
x2=[40 60 80 40 60 80 40 60 80 40 60 80];   %Wall thickness [0.001 in]
yd=[34.40 42.87 49.32 20.42 25.71 32.56 7.79 14.42 24.07 3.40 10.69 17.17];
%Damping (verify element 1)

[xData, yData, zData] = prepareSurfaceData( x1, x2, yd );

% Set up fittype and options.
ft = 'cubicinterp';

% Fit model to data.
[fitresult, gof] = fit( [xData, yData], zData, ft, 'Normalize', 'on' );

% Create a figure for the surface.
figure( 'Name', 'Damping Surface Regression' );
% Plot fit with data.
h = plot( fitresult, [xData, yData], zData );
% legend( h, 'Damping', 'yd vs. x1, x2', 'Location', 'NorthEast',
'Interpreter', 'none' );
% Label axes
```

```
xlabel( 'x1', 'Interpreter', 'none' );
ylabel( 'x2', 'Interpreter', 'none' );
zlabel( 'yd', 'Interpreter', 'none' );
grid on
view(45,30)

% Make contour plot.
figure( 'Name', 'Damping Contour' );
v=[0,5,10,15,20,25,30,35,40,45,50];
h = plot( fitresult, [xData, yData], zData, 'Style', 'Contour' );
h(1).LevelList=v;
h(1).ShowText='on';
h(1).LineWidth=1.5;
h(2).Marker='o';
h(2).Color=[0 0 0];
h(2).MarkerFaceColor=[0 0 0];
h(2).MarkerEdgeColor=[0 0 0];
h(2).MarkerSize=4;

grid on
title('Damping Contour')
xlabel('Cell size
(0.01")','FontWeight','normal','horizontalAlignment','center')
ylabel('Wall Thickness
(0.001")','FontWeight','normal','horizontalAlignment','center')
```

APPENDIX C. MANUFACTURING SUPPLEMENT

Basin Method for Foam Application

Equipment:

- SmoothOn Flex Foam-iT! 6
- 20 mL syringes (x2)
- 1 mixing cup
- 1 mixing stick (popsicle stick works well)
- Silicon Tubing (5/16" OD, 3/16" ID)
- 2 plexiglass plates at least 5"x5.5"
    - One plate should have holes drilled to line up with the honeycomb cells
- Multipurpose silicon lubricating grease
- 3D printed basin
- 3D printed pins (x13)
- Nitrile gloves
- Safety glasses
- Hot glue
- Clamps (x4)

Procedure:

1. Prepare top plexiglass plate by drilling small vent holes in the pattern of the desired honeycomb sample
2. 3D prints
    a. Print basin so that shock absorber fits snugly inside and sticks above the basin slightly (0.02").
    b. Print pins to exactly the size of the pin holes
3. Insert pins into the pin holes of the shock absorber
4. Hot glue the perimeter of the basin to the plexiglass plate without the holes (bottom plate)
5. Using a gloved finger, spread lubricating grease on the plexiglass inside of the basin. Also rub grease on the top plexiglass plate surface that will contact the foam
6. Cut 2 pieces of tubing approximately 3-4" each and insert them into the Luer lock fittings of the syringes. These are used as straws, so the syringes don't have to be dipped into the liquid obscuring the volume readings on the syringe.
7. Use the two syringes to suck up equal parts (about 15 mL) of Part A and Part B of the Flex Foam-iT kit (one syringe per Part). Actual volume needed depends on the geometry and the volume to be filled. It's better to overestimate because the excess will escape out of the drilled holes.

Steps 8-12 must be completed in approximately 30 seconds

8. Empty both syringes into the mixing cup and stir with the popsicle stick for approximately 15 seconds or until mixture appears homogeneous.
9. Pour mixture into the basin and help it to spread evenly until it covers the bottom of the basin. Tilting and blowing air are the most effective methods.

10. Press the honeycomb shock (with pinholes plugged) into the basin with the liquid mixture.
11. Align the top plexiglass plate so that the ventholes line up with all of the honeycomb cells
12. Clamp the plates together in such a way to distribute the pressure on the top plate evenly while not covering any of the vent holes
    a. Inadequate pressure on the top plate will allow foam to leak between cells underneath the top plate
13. Allow foam to cure for 2 hours
14. Unclamp plates and twist/peel off top plate
15. Use a XACTO knife to cut the hot glue and remove the basin from the bottom plate
16. Press the sample to remove it from the basin.
17. Push out the pins using a screwdriver or something similar
18. Clean up the shock by scraping away excess foam
19. Each cell will have a little knob of foam on the top side that comes from the foam inside the venthole. Use wire cutters or something similar to snip that knob and get a smooth surface for each cell
20. Peel off the excess foam that escaped through the vent holes in the top plate
21. Clean plexiglass. Use tweezers to clean vent holes of cured foam. Isopropyl alcohol takes foam residue right off. DO NOT USE ACETONE!
22. Clean or throw away syringes and silicon tubing
23. Basin and pins may be able to be used again depending on their condition
24. Throw away cup, mixing stick, paper towels, gloves, etc.

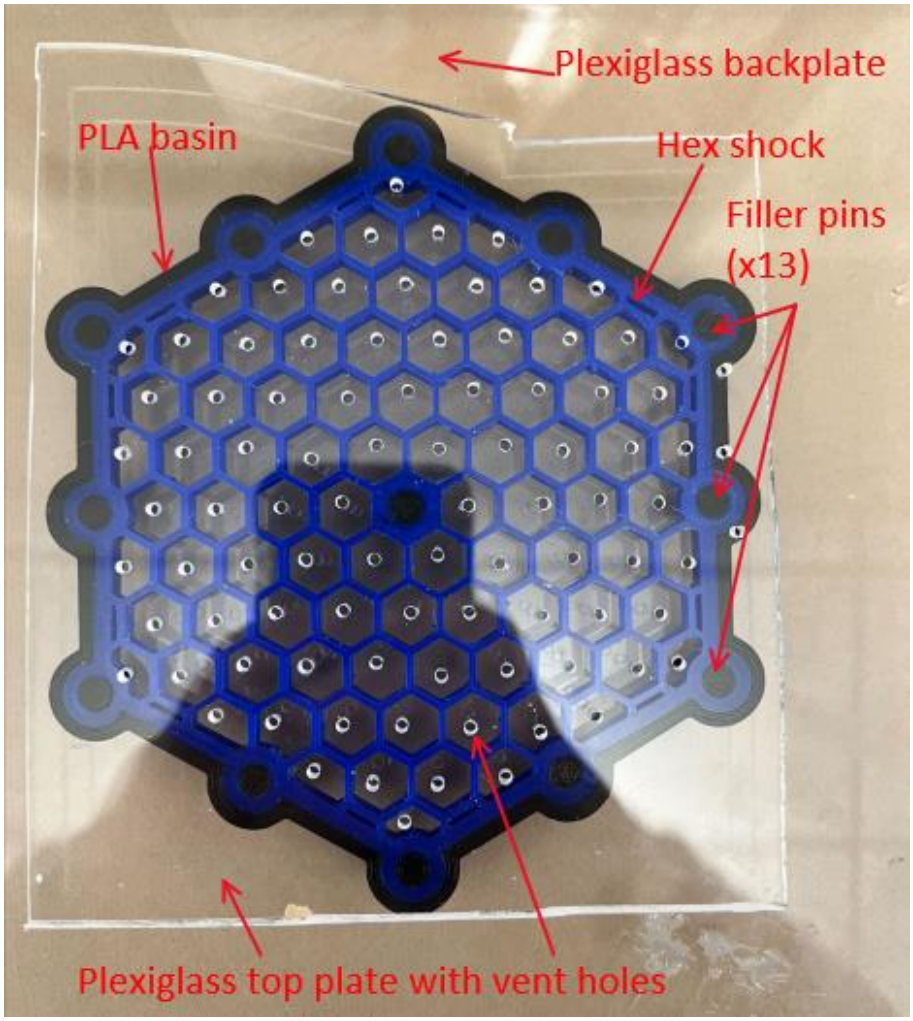

Figure C.1. Basin method setup diagram

Figure C.2. Multi-purpose silicone grease

APPENDIX D. TESTING SUPPLEMENT

Other shock absorber geometries were designed and tested. Ultimately, the honeycomb sample was selected because the honeycomb cells were easy to fill with foam and the mechanical properties of this design were the least dependent on strain rate.

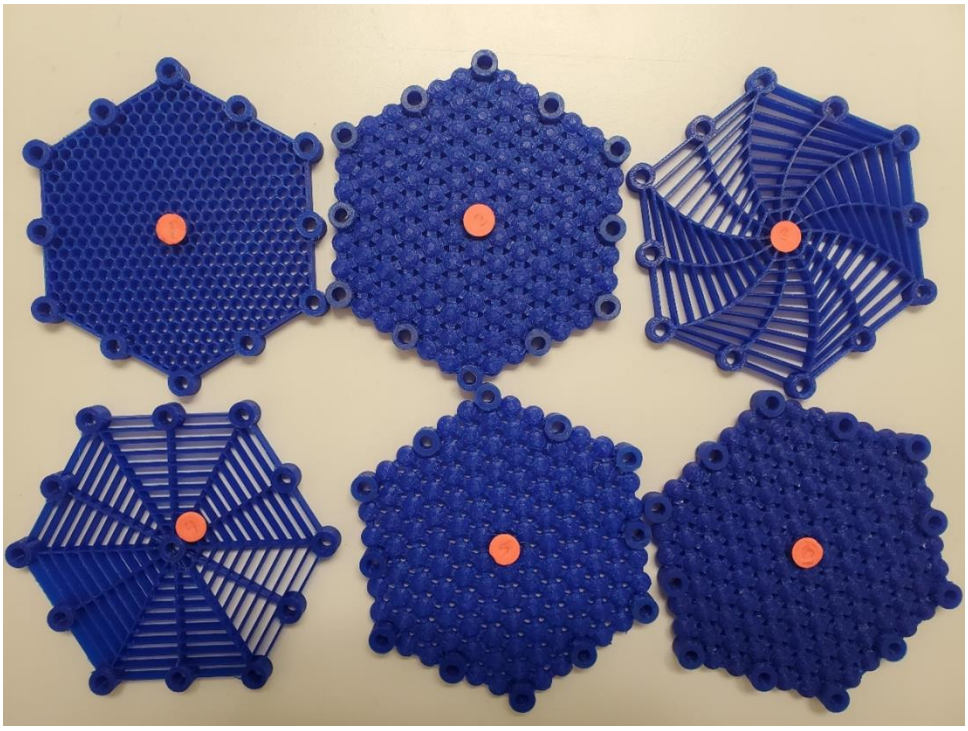

Figure D.1. Other sample geometries designed and tested.

The LabView program that controls the test machine is titled “288_003_Main_v4”. The front panel of this program is shown in Figure D.2.

List of Button Functions:
A Lock: Twists the actuator to lock the impactor mass to the pneumatic actuator
A Load: Manual retraction of the actuator. If the impactor mass is locked, the springs will load.
B Release: Manual release (forward) of the actuator. Impacting mass will not release.
Start Actuator Load: Automatic load of actuator until the rear proximity sensor is triggered
Start Release: Automatic release of the actuator until the front proximity sensor is triggered
Launch and Begin Measurement: The locking mechanism is released, and the program prepares to record data. The start of data collection is triggered by the second photogate.
Save Data: When on, the program will automatically write data to the file specified in the block diagram. Still requires user input to name each file. (Naming sequence: load cell, LVDT, velocity data)

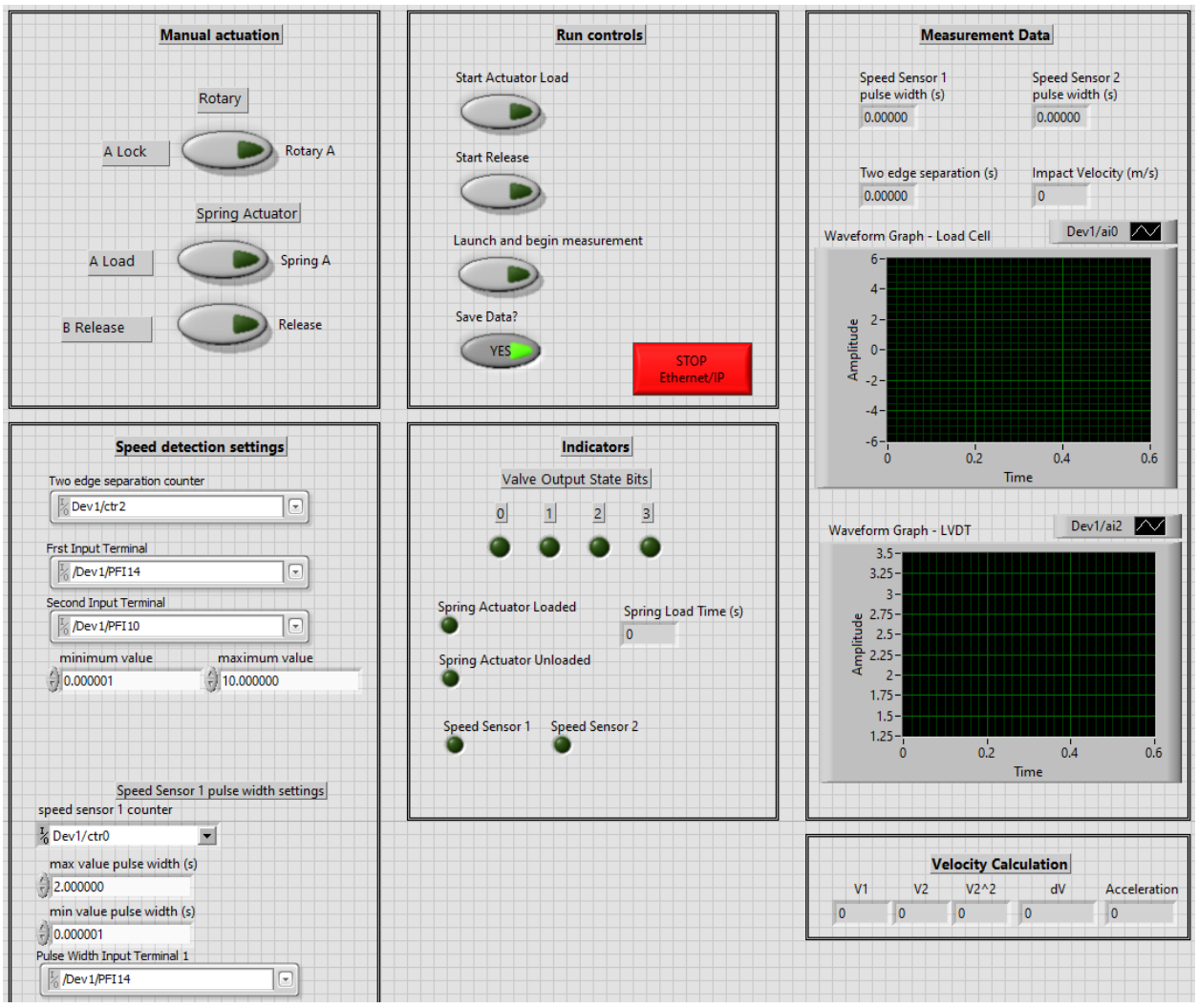

Figure D.2. LabView front panel of the control program for the machine.

Procedure to run a test:

1. Place sample onto pins in the bottom plate of sample holder. Slide the top plate of the sample holder over the top of the sample while guiding the LVDT rod into its cylinder.
2. Line up the hole in the top plate with the center pin hole of the sample. Screw the pin into top plate which should enter the center pin hole.
3. If you want to save the test data, make sure the “Save Data?” button is illuminated. Make sure to define the desired file path in the block diagram.
4. Ensure the pneumatic actuator is forward to start position (touching the yellow plate). If not, run the LabView program (Ctrl+R) and press “Start Release”. The actuator should stop when the front proximity sensor is triggered (barely touching the yellow plate).
5. Slide the impacting mass on the rail back into the pneumatic actuator. Insert the male end of the impactor into the female end of the actuator.
6. With the program running, press “A Lock” and wait for the lock to stop turning.
7. Press “Start Actuator Load” and wait for the actuator to load the springs and come to a stop.

8. Ensure nothing is in the travel path of the impacting mass and press “Launch and Begin Measurement”.
9. If “Save Data?” is enabled, then name the files in order as follows.
    a. “Load Cell Test #”
    b. “LVDT Test #”
    c. “Velocity Test #”
10. Press “Start Release” to begin unloading the actuator and returning it to the start position.
11. The saved data will be in “.lvm” file format. These files must be converted to “.txt” files to work with the Matlab functions. Total Commander is an easy way to rename all files at once.

Common Issues:

- If the program runs too long before a test is run, the “Launch and Begin Measurement” button may not work. Simply stop and restart the program.
- If you stop the program and then try to restart it too quickly, it will throw an error. Just stop the program again and wait a few seconds before starting it.
- The bearings for the sliders are run dry for increased speed. This accelerates the wear on the bearing and reduces life. If errors are observed, investigate this as a cause.

APPENDIX E. CUSTOM TESTING MACHINE INFORMATION

Hardware Specifications

- LVDT: Omega LD621A-50
  - Range: 0-50 mm
  - Output Voltage: 0-10 Vdc
  - Sensitivity: 1.7443 V/cm (calculated experimentally)

- Load Cell: Kistler Type 9323A, SN: 5717254
  - Range: 0-20 kN

- Actuator: SMC Pneumatics MGPMF80TN-175Z-M9P

- Slider Bearings: THK HSR25C

Pictures

Figure E.1. Electronics box

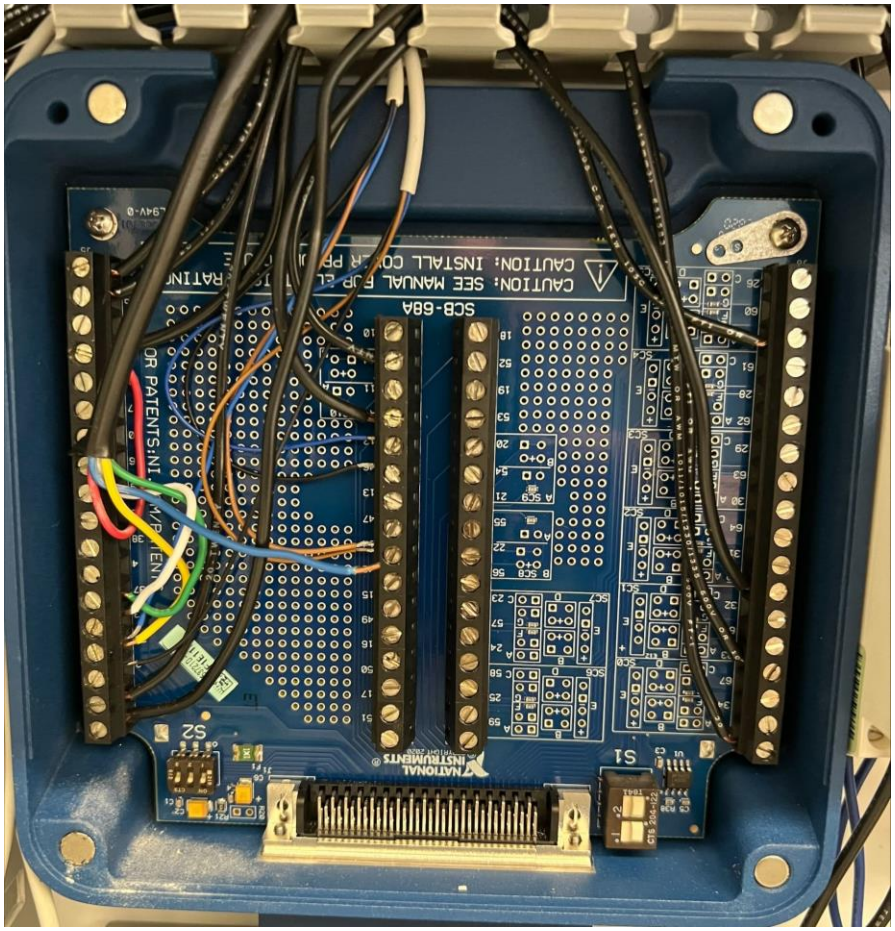

Figure E.2. NI DAQ wiring

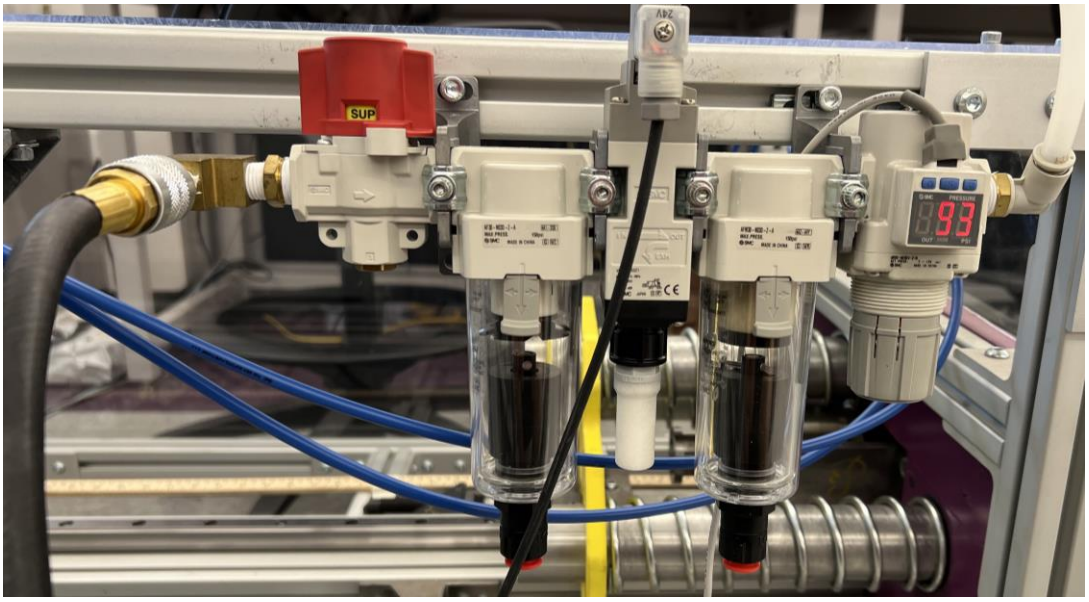

Figure E.3. Pressure regulator connected to facility compressed air line

REFERENCES

[1] T. Malik, "Space Station Astronaut Ready for Boston Marathon," Space.com, 04 April 2007. [Online]. [Accessed 22 June 2022].

[2] E. Callaway and A. Katsnelson, "How to keep the effects of environmental bounce out of your data," *TheScientist,* vol. 21, no. 9, 2007.

[3] M. Munk and M. Cagle, "Hypersonic Inflatable Aerodynamic Decelerator (HIAD)," National Aeronautics and Space Administration, 28 January 2021. [Online]. [Accessed 22 June 2022].

[4] Brain Injury Research Institute, "Protect the Brain," Brain Injury Research Institute, 2022. [Online]. Available: www.protectthebrain.org. [Accessed 3 May 2022].

[5] Mayo Clinic Staff, "Concussion," Mayo Clinic, 17 February 2022. [Online]. [Accessed 20 June 2022].

[6] D. F. Meaney and D. H. Smith, "Biomechanics of Concussion," *Clinics in Sports Medicine,* vol. 30, no. 1, pp. 19-31, 8 April 2011.

[7] F. Mesfin, N. Gupta and e. a. Hays Shapshak A, "Diffuse Axonal Injury," StatPearls Publishing, Treasure Island, 2021.

[8] D. Balandin, N. Bolotnik, J. Crandall, W. Pilkey and S. Purtsezov, "Optimal Impact Isolation for Injury Prevention Evaluated by the Head Injury Criterion," *Shock and Vibration*, no. 14, pp. 355-370, 2007.

[9] Biomechanics Consulting & Research, LLC (Biocore), "Helmet Test Protocol," Biocore LLC, Charlottesville, 2019.

[10] L. F. Gabler, J. R. Crandall and M. B. Panzer, "Development of a Second-Order System for Rapid Estimation of Maximum Brain Strain," *Annals of Biomedical Engineering,* vol. 47, no. 9, pp. 1971-1981, 2019.

[11] National Highway Traffic Safety Administration, *49 CFR Part 572: ANTHROPOMORPHIC TEST DEVICES,* 2011.

[12] I. Kaleps and J. Whitestone, "Hybrid III Geometrical and Inertial Properties," *SAE Transactions,* vol. 97, pp. 107-127, 1988.

[13] National Institute of Standards and Technology, "Central Composite Designs (CCD)," National Institute of Standards and Technology. [Online]. [Accessed 22 February 2022].

[14] J. J. Schwartz, J. Hamel, T. Ekstrom, L. Ndagang and A. J. Boydston, "Not all PLA filaments are created equal: an experimental investigation," *Rapid Prototyping Journal*, vol. 26, no. 7, pp. 1263-1276, 2020.

[15] Sorbothane, Incorporated, "Engineering Solutions Showcase," Sorbothane, Inc. [Online]. [Accessed 28 March 2022].

[16] E. J. Pellman, D. C. Viano, C. Withnall, N. Shewchenko, C. A. Bir and P. D. Halstead, "Concussion in professional football; helmet testing to assess impact performance - part 11," *Neurosurgery*, vol. 58, no. 1, pp. 78-96, 2006.

[17] A. M. Bailey and e. al., "Development and Evaluation of a Test Method for Assessing the Performance of American Football Helmets," *Annals of Biomedical Engineering*, vol. 48, no. 11, pp. 2566-2579, 2020.

[18] L. Zhang, K. Yang and T. A. Gennarelli, "Mathematical Modeling of Cerebral Concussion: Correlations of Regional Brain Strain with Clinical Symptoms," in *IRCOBI*, Bern (Switzerland), 2008.

[19] K. H. Y. Albert I King, L. Zhang and W. Hardy, "Is Head Injury Caused by Linear or Angular Acceleration?," in *IRCOBI*, Lisbon (Portugal), 2003.

[20] S. Rowson, G. Brolinson, M. Goforth, D. Dietter and S. Duma, "Linear and angular head acceleration measurements in collegiate football," *Journal of Biomechanical Engineering*, vol. 131, no. 6, 2009.

[21] Ruiz Brothers, "3D Printing with NinjaFlex," Adafruit Learning System, 7 February 2014. [Online].

[22] S. Renganathan, "Flexible Filaments for 3D Printing - Simply Explained," All3DP, 20 October 2020. [Online].

[23] A. Post, A. Oeur, B. Hoshizaki and M. D. Gilchrist, "An examination of American football helmets using brain deformation metrics associated with concussion," *Materials & Design*, vol. 45, pp. 653-662, 2013.

[24] MatterHackers, "Dremel DigiLab 3D45 3D Printer," MatterHackers. [Online]. [Accessed 24 June 2022].

VITA

Chase LeMaire is a Louisiana native who has always had a dream of graduating from Louisiana State University (LSU). His fascination with invention has been present from a young age, and he naturally gravitated toward engineering to obtain the knowledge necessary to bring his ideas to life. There are no engineers in his family, so it was sometimes challenging finding his way without any familial role models in the field. He even received some concern from his family because they did not want him constrained to a refinery or chemical plant as they have been their entire lives. They were unaware of the other opportunities that engineering offers, something that Chase had to discover for himself while blazing his own trail. In his time at LSU, Chase earned a position on the President's List (4.0+ GPA and 15+ hours) for 7 semesters. He graduated first in his class in Mechanical Engineering and second in the College of Engineering with a GPA of 4.221. Chase was also recognized as a University Medalist which is only awarded to students who have made straight A's throughout their entire college career. After four years of dedication, in May 2021, Chase graduated with a bachelor's degree in Mechanical Engineering from LSU and became the first engineer in his family. He was offered and accepted a position in the Accelerated Master's in Mechanical Engineering Program (Accel MSME) which will allow him to complete a master's in Mechanical Engineering with an anticipated graduation date of August 2022. Chase has accepted a position as an RF Mechanical Design Engineer with Raytheon Missiles and Defense and will relocate to Tucson, Arizona upon completion of his master's program.